Hopf saddle-node bifurcation for fixed points of 3D-diffeomorphisms: Analysis of a resonance 'bubble'

Henk Broer[a], Carles Simó[b], Renato Vitolo[c,*]

[a] *Department of Mathematics, University of Groningen, PO Box 800, 9700 AV Groningen, The Netherlands*
[b] *Dept. de Matemàtica Aplicada i Anàlisi, Universitat de Barcelona, Gran Via 585, 08007 Barcelona, Spain*
[c] *Dip. di Matematica ed Informatica, Università degli Studi di Camerino, via Madonna delle Carceri, 62032 Camerino, Italy*

Abstract

The dynamics near a Hopf saddle-node bifurcation of fixed points of diffeomorphisms is analysed by means of a case study: a two-parameter model map G is constructed, such that at the central bifurcation the derivative has two complex conjugate eigenvalues of modulus one and one real eigenvalue equal to 1. To investigate the effect of resonances, the complex eigenvalues are selected to have a 1:5 resonance. It is shown that, near the origin of the parameter space, the family G has two secondary Hopf saddle-node bifurcations of period five points. A cone-like structure exists in the neighbourhood, formed by two surfaces of saddle-node and a surface of Hopf bifurcations. Quasi-periodic bifurcations of an invariant circle, forming a frayed boundary, are numerically shown to occur in model G. Along such Cantor-like boundary, an intricate bifurcation structure is detected near a 1:5 resonance gap. Subordinate quasi-periodic bifurcations are found nearby, suggesting the occurrence of a cascade of quasi-periodic bifurcations.
© 2008 Elsevier B.V. All rights reserved.

Keywords: Quasi-periodic bifurcations; Two-torus attractor; 3D diffeomorphisms

1. Introduction

The goal of the present paper is to understand the typical bifurcation patterns organized around a Hopf saddle-node (HSN) bifurcation of fixed points, by means of a case study. To this end, a suitable parameterized family G of 3D maps is examined: at the origin of the parameter space, G has a fixed point such that the derivative of G at this fixed point has two complex conjugate eigenvalues of modulus one and one real eigenvalue equal to 1. Specifically, the issue is investigated of the effect of the resonances of the complex eigenvalues. Therefore, the complex eigenvalues at the fixed point are chosen as fifth roots of unity, which is the strongest among the weak resonances. Correspondingly, the model map G is constructed to be 'as generic as possible' in the class of diffeomorphisms unfolding a HSN bifurcation in the neighbourhood of a 1:5 resonance.

It is shown that the family G has two secondary Hopf saddle-node bifurcations of period five points near the origin of the parameter space. The Hopf saddle-node bifurcations organize a cone-like structure in parameter space, formed by two surfaces of saddle-node and a surface of Hopf bifurcations. Several conjectural results are presented on the basis of preliminary numerical results. Among the detected phenomena there is an intricate bifurcation structure near a 1:5 resonance gap, which occurs along a frayed boundary of quasi-periodic Hopf bifurcations of an invariant circle. Several bifurcations of invariant circles and two-tori

---

* Corresponding address: School of Engineering, Computing and Mathematics, University of Exeter, Harrison building, North Park Road, Exeter, EX4 4QF, United Kingdom. Tel.: +44 (0)1392 725280; fax: +44 (0)1392 264067.

E-mail addresses: H.W.Broer@math.rug.nl (H. Broer), carles@maia.ub.es (C. Simó), r.vitolo@exeter.ac.uk, renato.vitolo@unicam.it (R. Vitolo).

occur nearby, yielding a sort of cascade of quasi-periodic bifurcations and various pictorial configurations in phase space (more on the latter aspect will be reported in [17]).

We now introduce the definition of HSN bifurcation for maps. Let $\alpha \in \mathbb{R}^p$ be a multi-parameter, and denote by $\mathbb{S}^1 = \mathbb{R}/2\pi \subset \mathbb{C}$ the unit circle. Let $F_\alpha : \mathbb{R}^3 \to \mathbb{R}^3$ be a C^∞-family of diffeomorphisms. We say that F_α is an *HSN-family of diffeomorphisms* if

$$F_0(0) = 0, \quad \text{and} \quad \text{spec } DF_0(0) = \{e^{i\omega_0}, e^{-i\omega_0}, 1\} \subset \mathbb{S}^1, \tag{1}$$

where the complex conjugate eigenvalues satisfy the nonresonance conditions

$$e^{in\omega_0} \neq 1 \quad \text{for } n = 1, 2, 3, 4. \tag{2}$$

Remarks 1. 1. To have a HSN bifurcation, certain generic conditions on a finite jet of the map F are required (namely, Eqs. (37) and (38) in Appendix A.1).
2. In the k-dimensional case with $k > 3$, explicit formulas for the critical coefficients of the Poincaré normal form (Eq. (40) in Appendix A.1) in the 3D-centre manifold for the HSN bifurcation are given in [49]. Computation of these coefficients has been implemented in the standard bifurcation software MatCont [36]. For clarity, we also emphasize that the term "HSN bifurcation" as defined here and in [16,66,67] is a synonym for fold-Neĭmark–Sacker[1] bifurcation as defined in [36,48–50].
3. A HSN bifurcation of fixed points is one of the organizing centres of the bifurcation diagram of a diffeomorphism arising in the study of a climatological model, see [15] and [66, Chap 2].
4. The values $n = 1, 2, 3, 4$ in Eq. (2) are the so-called strong resonances [3,61,48]. They are excluded since we wish to keep the normal form free from resonant terms (that is, axially symmetrical) up to order 3 (see Lemma 6).

The parameterized model family G considered here is

$$G : \begin{pmatrix} w \\ z \end{pmatrix} \mapsto \begin{pmatrix} e^{i(\omega_0 + \gamma\delta)}w[1 - \gamma(\gamma\mu + az + \gamma z^2)] \\ z + \gamma(1 - |w|^2 - z^2) \end{pmatrix} + \begin{pmatrix} \gamma^3(\varepsilon_1 \overline{w}^4 + \varepsilon_2 z^4) \\ 0 \end{pmatrix}. \tag{3}$$

The family G depends on the three real parameters (γ, μ, δ), and is given in the coordinates (w, z), where $w = x + iy \in \mathbb{C}$ and $z \in \mathbb{R}$. The coefficients $a = a_1 + ia_2 \in \mathbb{C}$, $\varepsilon_j \in \mathbb{R}$, $j = 1, 2$ are constants belonging to a fixed compact set, while ω_0 is fixed at $2\pi/5$ throughout the paper.

The present paper contains a summary of analytical and numerical results concerning model map G, which is constructed to be 'as generic as possible' in the class of diffeomorphisms having a HSN bifurcation in the vicinity of a 1:5 resonance. A detailed dynamic analysis, based on numerical tools, is in preparation [17], also see [66, Chap 4].

An outline of the present paper follows. In Section 2 we sketch the construction of the model map G, referring to [66, Sec. 4.1.2] for more details. Analytical results on the bifurcation diagram of G are given in Section 3 (for readability, all proofs are postponed to Appendices A and B). A brief summary of the many, intricate phenomena observed numerically for map G is presented in Section 4, whereas ongoing research and open problems are discussed in the conclusions (Section 5).

All software for the numerical computations (calculation of Lyapunov exponents, computation and continuation of fixed and periodic points, invariant curves, bifurcation diagrams, etc.) has been produced by the authors in the most efficient and accurate way, taking into account the particular properties of the models under study.

2. Model setup and theoretical expectations

Given a family of diffeomorphisms F_α, $\alpha \in \mathbb{R}^p$, a standard approach for the study of a bifurcation of fixed points of F_α consists in the analysis of the Takens normal form vector field, see [61] and Appendix A.2. To briefly summarize this, let $DF_0(0) = S + N$ be the decomposition in semisimple and nilpotent part of $DF_0(0)$. By Takens's theorem there exists a change of coordinates, defined in a neighbourhood of the origin of $\mathbb{R}^3 \times \mathbb{R}^p$ and preserving the parameters, such that in the new coordinates the diffeomorphism F_α takes the form

$$F_\alpha = S \circ X_\alpha^1 + M,$$

where the Taylor expansion of the remainder M near the origin is identically zero. Here X_α^1 denotes the time-1 map of a family of vector fields X_α, defined on $\mathbb{R}^3$ and such that

$$X_0(0) = 0 \quad \text{and} \quad \text{spec } DX_0(0) = \{0\}.$$

However, if F is an HSN-family of diffeomorphisms, the following version of Takens's theorem holds.

---

[1] Ruelle and Takens [57] use the term "Hopf bifurcation" for fixed points, but acknowledge in a footnote that Neĭmark and Sacker had studied it first.

Theorem 1. *Let $F_\alpha : \mathbb{R}^3 \to \mathbb{R}^3$ be a smooth HSN-family of diffeomorphisms, depending on the parameter $\alpha \in \mathbb{R}^3$. Suppose that F_α satisfies certain open and dense conditions (specified in the proof of the Theorem, see Appendix B). Then there exist a smooth parameter-dependent transformation and a reparameterization $\beta = (\beta_1, \beta_2, \delta)(\alpha)$ such that, by denoting $F_{\beta_1, \beta_2, \delta}$ the map F_α expressed in the new parameters and coordinates, one has*

$$F_{\beta_1, \beta_2, \delta}(w, z) = Z^1_{\beta_1, \beta_2, \delta}(w, z) + \mathcal{O}(\|w, z\|^4), \tag{4}$$

with $w \in \mathbb{C}$ and $z \in \mathbb{R}$. Here $Z^1_{\beta_1, \beta_2, \delta}$ is the time-one map of the flow of the third degree polynomial vector field

$$Z_{\beta_1, \beta_2, \delta}(w, z) = \begin{pmatrix} (\beta_2 + i(\omega_0 + \delta))w + awz + bwz^2 \\ \beta_1 + sw\overline{w} + z^2 + cz^3 \end{pmatrix}, \tag{5}$$

where $s = \pm 1$ and a, b, c are functions of the parameters $(\beta_1, \beta_2, \delta)$ such that $a, b \in \mathbb{C}$ and $c \in \mathbb{R}$.

This theorem forms the basis of our construction of the 'generic' model map G (3). The vector field $Z_{\beta_1, \beta_2, \delta}$ is a truncated normal form for the HSN bifurcation of equilibria of vector fields. This normal form is obtained by only using near-identity transformations, followed by a scaling of the phase variables and a change of parameters. In fact, by also applying two scalings of time, it can be shown [48, Lemma 8.11] that a simpler vector field $Y_{\beta_1, \beta_2, \omega}$ can be obtained

$$Y_{\beta_1, \beta_2, \omega}(w, z) = \begin{pmatrix} (-\beta_2 + i\omega)w - awz - wz^2 \\ -\beta_1 - sw\overline{w} - z^2 \end{pmatrix}, \tag{6}$$

with $a = a(\beta_1, \beta_2, \omega) \in \mathbb{C}$ and $s = \pm 1$. In few words, the construction of model map G (3) runs as follows: we start from the vector field $Y_{\beta_1, \beta_2, \omega}$ in (6), apply a parameter transformation and a scaling of time and variables, compute an (approximate) time-1 map and add certain perturbative terms of order four to destroy the axial symmetry of the vector field $Y_{\beta_1, \beta_2, \omega}$ (see the next section). By (4), this construction is likely to be representative for a large class of HSN-diffeomorphisms. Since our construction focuses on dynamic phenomena occurring in a specific region of the (β_1, β_2)-parameter plane, the bifurcation diagram of the vector field $Y_{\beta_1, \beta_2, \omega}$ is briefly recalled in the next subsection.

2.1. Dynamics of Hopf saddle-node vector fields

The Hopf saddle-node bifurcation of equilibria of vector fields has been investigated by several authors [8,18,21,25,28,34,37,44,47,48,63]. To introduce the notation used in this paper and to illustrate the problem setting, we briefly recall the main features.

Let X_α be a C^∞-family of vector fields on $\mathbb{R}^3$, where $\alpha \in \mathbb{R}^p$ is a multi-parameter. We call X_α a *HSN-family of vector fields* if

$$X_0(0) = 0 \quad \text{and} \quad \text{spec } DX_0(0) = \{\pm i\nu_0, 0\}, \quad \nu_0 \neq 0.$$

To have a generic HSN bifurcation of equilibria, the 3-jet of X_α at the origin has to satisfy appropriate open and dense conditions, *e.g.* those given in [48, Lemma 8.11]. Under the latter conditions, there exist a sequence of coordinate transformations, time scalings and a final reparameterization such that, by denoting X_β the vector field X_α written in the new coordinates, time and parameters, we have

$$X_\beta(w, z) = Y_{\beta_1, \beta_2, \omega} + \mathcal{O}(\|w, z\|^4), \tag{7}$$

where $Y_{\beta_1, \beta_2, \omega}$ is the vector field in (6). We emphasize that in the vector field case, since one usually works modulo orbital equivalence (time scalings are allowed), ω may be assumed to be a nonzero constant. In other words, the "detuning" parameter δ contained in $Z_{\beta_1, \beta_2, \delta}$ (5) is not needed: only two control parameters are used, therefore we take $\alpha \in \mathbb{R}^p$ with $p = 2$. Correspondingly, only the parameters β_1 and β_2 are considered in the bifurcation analysis.

Since $Y_{\beta_1, \beta_2, \omega}$ is *axially symmetrical*, by using cylindrical coordinates (r, ϕ, z), where $w = re^{i\phi}$, and disregarding the ϕ-component (since the (r, z)-components are independent on ϕ), we obtain the planar reduction

$$\begin{aligned} \dot{r} &= r(-\beta_2 - a_1 z - z^2), \\ \dot{z} &= -\beta_1 - z^2 - sr^2, \end{aligned} \tag{8}$$

where a_1 is the real part of the coefficient a in (6). The vector field (8) is $\mathbb{Z}_2$-equivariant, namely, it is symmetrical under the transformation $(r, z) \mapsto (-r, z)$.

According to the signs of s and a_1, the topological structure of the phase portrait of the reduced system (8) belongs to one of four classes (if a time-reversal is allowed [48]). The unfolding case of present interest is $s = 1$, $a_1 < 0$, see Fig. 1, for which both Hopf
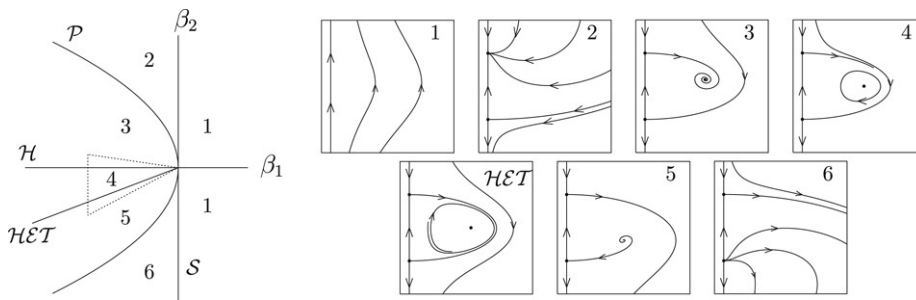
Fig. 1. Unfolding of the HSN bifurcation for vector fields: bifurcation diagram of the planar system (8) in the case $s = 1$, $a_1 < 0$, from [48, Section 8.5]. Phase portraits in the (r, z)-plane are given on the right.

and heteroclinic bifurcations occur. The bifurcation diagram of the planar system (8) consists of the curves $\mathcal{S}$, $\mathcal{P}$, $\mathcal{H}$ and $\mathcal{HET}$:

$$\mathcal{S} = \{(\beta_1, \beta_2) \mid \beta_1 = 0\}$$
$$\mathcal{P} = \left\{(\beta_1, \beta_2) \mid \beta_1 = -\frac{\beta_2^2}{a_1^2} + o(\beta_2^2)\right\}$$
$$\mathcal{H} = \{(\beta_1, \beta_2) \mid \beta_1 < 0, \beta_2 = 0\}$$
$$\mathcal{HET} = \left\{(\beta_1, \beta_2) \mid \beta_1 < 0, \beta_2 = \frac{a_1}{3a_1 - 2}\beta_1 + o(\beta_1)\right\}.$$

Compare Fig. 1, where we also indicate the phase portraits of the planar system system (8). Saddle-node, pitchfork, and (Andronov-) Hopf bifurcations of equilibria take place for parameters on the curves $\mathcal{S}$, $\mathcal{P}$, and $\mathcal{H}$ respectively, while $\mathcal{HET}$ is a curve of heteroclinic bifurcations of equilibria. Two equilibria $\mathcal{O}_\pm = (\pm\sqrt{-\beta_1}, 0)$ exist in regions 2 up to 6. In regions 3, 4, and 5 the equilibria $\mathcal{O}_\pm$ are of saddle type and have a one-dimensional heteroclinic connection along the z-axis. This connection is persistent in (8) due to the $\mathbb{Z}^2$-symmetry. Furthermore, a third equilibrium $\mathscr{C}$ coexists with $\mathcal{O}_\pm$ in regions 3, 4, 5. The equilibrium $\mathscr{C}$ is attracting in region 3 and repelling in regions 4 and 5. Entering region 4 from region 3 across curve $\mathcal{H}$, the equilibrium $\mathscr{C}$ loses stability through a Hopf bifurcation, whereby an attracting limit cycle $\mathscr{T}$ is created. As (β_1, β_2) approach the curve $\mathcal{HET}$, the limit cycle $\mathscr{T}$ grows in size and in period. For $(\beta_1, \beta_2) \in \mathcal{HET}$, the limit cycle $\mathscr{T}$ turns into a heteroclinic connection formed by the z-axis and by the unstable manifold of $\mathcal{O}_+$, which has merged with the stable manifold of $\mathcal{O}_-$.

The dynamics of the three-dimensional polynomial family $Y_{\beta_1,\beta_2,\omega}$ is easily reconstructed from the dynamics of (8): for example, $\mathcal{H}$ becomes a Hopf (also called Neĭmark–Sacker [48]) bifurcation where a limit cycle, again denoted by $\mathscr{C}$, loses stability and an attracting two-torus $\mathscr{T}$ branches off. Then $\mathscr{T}$ merges into a heteroclinic sphere-like structure on the curve $\mathcal{HET}$. For a generic HSN-family of the form X_β (7), the local bifurcations $\mathcal{S}$, $\mathcal{P}$, and $\mathcal{H}$ are expected to persist, whereas the heteroclinic sphere splits into a transversal heteroclinic structure [8,19,21,44] and this allows the occurrence of Shil'nikov homoclinic bifurcations [8,21,34, 37,48]. The occurrence of Shil'nikov bifurcations implies that the germ of the vector field is not stable [18,62]. The torus $\mathscr{T}$ of X_β breaks down when approaching the heteroclinic structure. This phenomenon is only partially understood from the theoretical viewpoint [1,4,5,14,27,54]. For parameters inside a resonance tongue, homoclinic tangency bifurcations of periodic orbits lying inside $\mathscr{T}$ are often related to the breakdown of the torus and to the creation of strange attractors [37,44,48].

2.2. Construction of the model map

We start from vector field $Y_{\beta_1,\beta_2,\omega}$ (6), in the unfolding case $a_1 < 0$, $s = 1$. The area of interest in the (β_1, β_2)-parameter plane is bounded by a dashed triangle in Fig. 1 (left panel): it is a sector containing region 4 and parts of regions 3 and 5. Only negative values of β_1 are considered. New parameters (γ, μ) are introduced by

$$\beta_1 = -\gamma^2, \qquad \beta_2 = \gamma^2\mu, \tag{9}$$

where $\gamma > 0$ and $\mu \in \mathbb{R}$. The effect of this reparameterization is sketched in Fig. 2: the dashed sector in Fig. 1 (magnified in Fig. 2 left) is blown up near the origin and mapped onto a horizontal strip in the (γ, μ)-plane (Fig. 2 right). Thereby, the bifurcation curves $\mathcal{H}$ and $\mathcal{HET}$ both turn into horizontal lines in the (γ, μ)-parameter plane.

Remark 2. Notice that, for the model map, ω must be taken as a parameter together with (γ, μ). Indeed, for a HSN-family of vector fields, ω can be set to one by a time scaling, but this is not possible for a map.

Beyond the reparameterization (9), the variables and the time of (6) are rescaled as follows:

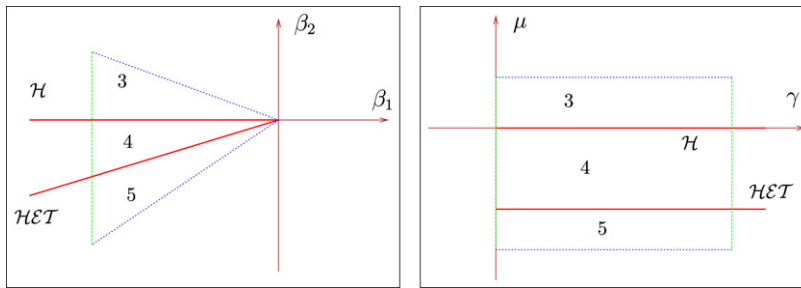$$w = \gamma\widehat{w}, \qquad z = \gamma\widehat{z}, \qquad t = \widehat{t}/\gamma. \tag{10}$$

Fig. 2. Left: magnification of Fig. 1 near the sector of interest in the (β_1, β_2)-parameter plane. Right: in the (γ, μ)-parameter plane, where (γ, μ) are given by the scaling (9), the sector of interest (left picture) is blown up near the origin.

The effect of this scaling is to keep the sizes of the limit cycle $\mathscr{C}$ and of the torus $\mathscr{T}$ of order $\mathcal{O}(1)$ as $\gamma \to 0$. Denote by $Y_{\gamma,\mu,\omega}$ the vector field in (6) written in the variables and parameters defined in (10) and (9). By dropping all hats, $Y_{\gamma,\mu,\omega}$ reads

$$Y_{\gamma,\mu,\omega} = Y_1 + Y_2, \quad \text{with } Y_1 = \begin{pmatrix} -\gamma\mu w - awz - \gamma wz^2 \\ 1 - z^2 - |w|^2 \end{pmatrix}, \qquad Y_2 = \begin{pmatrix} i\omega w/\gamma \\ 0 \end{pmatrix}. \tag{11}$$

The first step in the construction of the model map G (3) is to obtain an approximate time-γ map of the vector field $Y_{\gamma,\mu,\omega}$. Since Y_1 commutes with Y_2, the time-γ map of $Y_{\gamma,\mu,\omega}$ is given by the composition of the time-γ maps Y_1^γ and Y_2^γ (this is a corollary of the Baker–Campbell–Hausdorff formula [65]). So we first compute an *approximate* time-γ map of Y_1 by performing one step of length γ of the Euler integration formula

$$\begin{pmatrix} w \\ z \end{pmatrix} \mapsto \begin{pmatrix} w \\ z \end{pmatrix} + \gamma \begin{pmatrix} -\gamma\mu w - awz - \gamma wz^2 \\ 1 - z^2 - |w|^2 \end{pmatrix}. \tag{12}$$

Then the map (12) is composed with the time-γ map Y_2^γ, yielding the axially symmetrical map S:

$$S : \begin{pmatrix} w \\ z \end{pmatrix} \mapsto \begin{pmatrix} e^{i\omega} w[1 - \gamma(\gamma\mu + az + \gamma z^2)] \\ z - \gamma(-1 + |w|^2 + z^2) \end{pmatrix}. \tag{13}$$

The second and last step in the construction of the model map G is to add 'generic', nonaxisymmetrical resonant terms of order four (compare with Theorem 1) to map S. The choice of such terms depends on the resonant frequency ω_0 we wish to consider. In this paper we focus on the resonant value $\omega_0/(2\pi) = 1/5$, which is the lowest-order resonance compatible with the assumptions in (2). For this choice of ω_0, the lowest-order nonaxisymmetrical resonant terms in the $\partial/\partial w$ and in the $\partial/\partial z$-direction are $\overline{w}^4$ and $\mathrm{Re}\, w^5$, respectively. A further (nonresonant) term in z^4 is added to the w-component in order to break invariance of the z-axis. Moreover, a scaled detuning parameter δ is introduced, by setting $\omega = \omega_0 + \gamma\delta$. This yields the map

$$\begin{pmatrix} w \\ z \end{pmatrix} \mapsto \begin{pmatrix} e^{i(\omega_0 + \gamma\delta)} w[1 - \gamma(\gamma\mu + az + \gamma z^2)] \\ z - \gamma(-1 + |w|^2 + z^2) \end{pmatrix} + \begin{pmatrix} \gamma^3(\varepsilon_1 \overline{w}^4 + \varepsilon_2 z^4) \\ \gamma^4 \varepsilon_3 \, \mathrm{Re}\, w^5 \end{pmatrix}, \tag{14}$$

where ε_1 and ε_2 are complex while ε_3 is real. Notice that map G (3) is slightly simplified with respect to (14): ε_1 can be taken real, since a transformation of the form $(w, z) = R_\theta(w', z') = (\exp(i\theta)w', z')$ for suitable θ yields a system of coordinates where $\mathrm{Im}(\varepsilon_1) = 0$. Moreover, the parameter ε_3 is fixed at zero in G: this is reasonable, since the term in ε_3 of (14) is of order γ^4, while the $\partial/\partial z$-component of G already contains a term in γz^2. We refer to [66, App. 4.E] for a more detailed discussion on the choice of the values for the coefficients of G.

At this point it is worth adding a comment on the choice of Euler's explicit method to go from (12) to (13). Consider a planar conservative linear system like $\dot{x} = ax + by$, $\dot{y} = cx - ay$. The map induced by Euler's method with step size γ is linear and its matrix has determinant $1 - (a^2 + bc)\gamma^2$. Therefore, the numerical method produces an expansive (respectively, dissipative) map in the case that the origin is a centre (respectively, a saddle). Other integration methods have different behaviour around these points or the determinant differs from 1 by $O(\gamma^k)$, $k > 2$. On the invariant torus of vector field $Y_{\gamma,\mu,\omega}$, existing in region 4 of Fig. 2, the flow is close to conservative. When passing to the map we can have values of the parameters for which the two frequencies of the torus dynamics satisfy a double resonance condition. This gives rise to the existence of periodic points on the invariant torus. Were the map exactly conservative in the torus, generically half of the periodic points would be centres and the other half would be saddles. Using Euler's method the centres always become unstable foci: in this way it is prevented that they become attractors. On the other hand, the saddles become dissipative. If homoclinic tangles exist, this allows the possibility that strange attractors are created. For more details see [16].

2.3. Theoretical expectations

Having in mind the construction of the model map G (3), as well as the bifurcation diagram in Fig. 1, we can now describe which kind of dynamic phenomena we wish to analyse (and expect to find) in studying this map. Consider first the HSN family of diffeomorphisms $Y^1_{\beta_1,\beta_2,\omega}$, obtained by taking the time-1 map of the three-dimensional axially symmetric vector field (6). When β_2 decreases through zero between regions 3 and 4, $Y^1_{\beta_1,\beta_2,\omega}$ has a circle attractor with *parallel dynamics* (rigid rotation) that loses stability, whereby an invariant two-torus branches off. Moreover, on line $\mathcal{HET}$ there exists an invariant sphere formed by the stable and unstable manifolds of the polar saddle fixed points. This whole picture is very degenerate in the context of three-dimensional diffeomorphisms, but provides the geometrical skeleton of reference in our discussion, since by (4) the HSN families we consider are perturbations of $Y^1_{\beta_1,\beta_2,\omega}$. In particular, we here focus on three classes of dynamic phenomena that are expected to occur in generic HSN families of diffeomorphisms:

1. Interaction of resonances and the Hopf–Neĭmark–Sacker bifurcation.
2. Two-torus dynamics.
3. Two-torus breakdown and strange attractors near the heteroclinic region.

Let us briefly recall what is the generic expectation regarding the Hopf–Neĭmark–Sacker bifurcation. For a diffeomorphism (written as in (4)), this transition turns into a quasi-periodic Hopf bifurcation, where a circle attractor loses stability and a two-torus attractor branches off. This scenario has been described extensively by Broer et al. [7,9,10,26] as a part of dissipative KAM theory (also see [41] for a treatment specific of the HSN case). In this setting, resonances play a very strong role, since they involve a Cantor set of Diophantine conditions in the ω-direction. Summarizing, in parameter space we get a (Whitney) smooth foliation of positive measure, parameterized over the Diophantine Cantor set, where the smooth circle attractors lose stability and smooth two-torus attractors branch off. Both circles and two-tori are Diophantine, and hence form families of quasi-periodic attractors. The corresponding nowhere dense parameter regions with invariant circles and two-tori, by normal hyperbolicity can be extended to open subsets of parameter space (though not uniformly). Using the fact that quasi-periodic circles and two-tori are r-normally hyperbolic for any $r > 0$, this extension is considerable, just leaving out resonance gaps, called 'bubbles' [22–24], around most resonance points in the locus $\mathcal{H}$ of the Hopf bifurcations.

Inside the resonance 'bubbles' the rotation number of the circle, as far as it exists, is rational. Generically the corresponding circle dynamics is 'phase-locked' or 'Kupka-Smale', which means that the circle contains periodic points of saddle and of node type, where the circle itself is the closure of the union of unstable manifolds of the saddle points (see *e.g.* [3]). Closer to the locus $\mathcal{H}$ of Hopf bifurcations, the dynamics becomes more involved and generically one expects intricate patterns of secondary bifurcations, where the invariant circle does not always survive, but where transitions are possible to chaotic dynamics. (For similar scenario's for two-dimensional maps compare with, *e.g.,* [6,20,22–24,49,50,64,68,69]). Since the 1:5 resonance has lowest order amongst those compatible with (2), it is likely to have the strongest influence on the bifurcation diagram near $\mathcal{H}$. Therefore, the three-dimensional patterns of bifurcation near a 1:5 resonance are a main topic of the present research.

A second topic of interest is the organization of resonances for the dynamics inside the two-torus attractor that branches off at the quasi-periodic Hopf bifurcations belonging to $\mathcal{H}$. The two frequencies of the two-torus are resonant along open sets that form an intricate web in parameter space, particularly near resonance gap crossings, where strange attractors and cascades of quasi-periodic bifurcations may show up. Since this part of the investigation does not focus on the vicinity of a specific resonance along $\mathcal{H}$, wider domains in the ω-direction need to be examined.

A third and last point is the dynamics regarding the stable and unstable manifolds of the polar saddles ($\mathcal{O}_\pm$, compare Section 2.1) and the corresponding heteroclinic phenomena, which result in several types of strange attractors mostly involving the breakdown of the two-tori. In the present real analytic case, these hetero- and homoclinic phenomena are expected to occur in an exponentially narrow wedge in the parameter space [11–13,60].

Turning to our model map G (3), the above discussion is summarized in Fig. 3: the left panel contains the bifurcation diagram of the diffeomorphism $Y^1_{\gamma,\mu,\omega}$, given by the time-1 map of vector field family (11), inside the three-dimensional parameter space (γ, μ, ω); in the right panel we sketch our expectations for model map G. A number of theoretical results can be obtained for the vector field family $Y_{\gamma,\mu,\omega}$ (11) by invoking standard perturbation theory (normal hyperbolicity [33,40]) and quasi-periodic bifurcation theory [7,9,10,26]. The surface $\mathcal{HET}$ of heteroclinic bifurcations of the diffeomorphism $Y^1_{\gamma,\mu,\omega}$ turns into a region characterized by heteroclinic intersections of the polar saddle-like fixed points for the model map G [11–13,60]. As for the size of this region, we expect it to be exponentially narrow as $\gamma \downarrow 0$: here we use the real analyticity of the system and a refined averaging technique, which goes back on [52]. We refer to this part of the parameter space as the *heteroclinic region $\mathcal{HET}$*. Of the Hopf bifurcation surface $\mathcal{H}$, only a (Whitney) smooth Cantor foliation of lines (interspersed of resonance bubbles) survives for G: this is where there is a transition from the circle attractor to a circle repellor and a branching of a two-torus attractor (all of which are Diophantine). We refer to this frayed Cantor-like bifurcation set as the *Hopf bifurcation boundary $\mathcal{H}$*. $\mathcal{H}$ and $\mathcal{HET}$ roughly divide the parameter space into three regions, labelled by 3, 4 and 5. In region 3 (*i.e.*, for $\mu > 0$) there is a circle attractor $\mathcal{C}$. In region 4 (*e.g.,* for $\mu < 0$ and in between $\mathcal{H}$ and $\mathcal{HET}$) the circle $\mathcal{C}$ is repelling and it coexists with a two-torus attractor. The set $\mathfrak{A}^{p/q}$, consisting of all parameter values for which the rotation number on the invariant circle $\mathscr{C}$ is $p/q \in \mathbb{Q}$, is an Arnol'd resonance
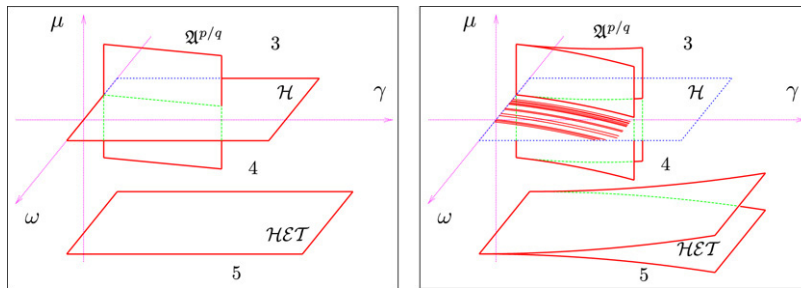
Fig. 3. Sketch of the theoretical expectations concerning the bifurcation structure of model map *G* (3) in the three-dimensional parameter space (γ, μ, ω). Left: bifurcation set of the HSN-family of maps $Y^1_{\gamma,\mu,\omega}$ given by the time-1 map of vector field (11) in the parameter region of our interest. $\mathfrak{A}^{p/q}$ is the set of all parameter values for which the rotation number on the invariant circle $\mathscr{C}$ is $p/q \in \mathbb{Q}$. See text for the meaning of $\mathcal{H}$ and $\mathcal{HET}$. Right: expected bifurcation set of the model map *G* (3), assuming genericity. $\mathfrak{A}^{p/q}$ is a resonance wedge of rotation number p/q, $\mathcal{HET}$ is an exponentially narrow wedge where heteroclinic intersections and tangencies occur. Of the surface $\mathcal{H}$, only a Cantor-like foliation by curves survives.

tongue. The intersection of this three-dimensional tongue with a vertical plane $\gamma = \mathrm{const.}$ yields a 1:5 resonance gap which extends further away from the 1:5 'bubble': the latter is confined near the Hopf bifurcation boundary $\mathcal{H}$.

We emphasize that Fig. 3 only provides a rough geometrical skeleton for the dynamics of the maps. Many issues need to be analysed by specific means. For instance, what is the fate of the invariant circle inside the 1:5 resonance 'bubble' near the Hopf bifurcation boundary $\mathcal{H}$? Which additional bifurcations of invariant circles and two-tori show up? What is the structure of the 1:5 resonance gap, further away from $\mathcal{H}$? Which are the typical routes to the formation of strange attractors near region $\mathcal{HET}$? The present paper contains a few analytical results concerning the bifurcation structure of model map *G* near the 1:5 resonance 'bubble'. This is a first analytical treatment of point 1 in the enumeration at the beginning of this section. Moreover, a brief illustration of the dynamic richness of *G* is given, by briefly discussing some numerical results. A comprehensive dynamic study of points 1, 2, 3, carried out by numerical means, is in preparation [17], also see [66, Chap 4].

We conclude by observing that the complexity of the present bifurcation can be easily met in concrete studies, *e.g.* see [15] where this and related problems are encountered in the dynamic modelling of the northern hemisphere climate.

3. Analytical study of the model map

In this section we discuss a few results concerning the bifurcation diagram of the model family *G* as in (3). First, by examining an axially symmetrical truncation of the map, analytical expressions are derived for the position of the Hopf bifurcation boundary and for the region of heteroclinic intersections depending on the perturbation parameter γ. Then, in Section 3.2, analogous expressions are given for the saddle-node, Hopf and Hopf saddle-node bifurcations of period five points of the map *G*. The latter are obtained by studying a suitable Takens normal form vector field. All proofs are given in the Appendix for better readability.

3.1. The axially symmetrical truncation

The model map *G* (3) is a perturbation of the axially symmetrical family *S* (13). In cylindrical coordinates (r, ϕ, z), where $w = r \exp(\mathrm{i}\phi)$, *S* reads

$$S : \begin{pmatrix} r \\ \phi \\ z \end{pmatrix} \mapsto \begin{pmatrix} r \left| 1 - \gamma(\gamma\mu + az + \gamma z^2) \right| \\ \phi + \omega + \arg(1 - \gamma(\gamma\mu + az + \gamma z^2)) \\ z - \gamma(-1 + r^2 + z^2) \end{pmatrix}. \tag{15}$$

Since the dynamics in the (r, z)-components is independent on ϕ, we consider the reduced planar map $\widetilde{S}$

$$\widetilde{S} : \begin{pmatrix} r \\ z \end{pmatrix} \mapsto \begin{pmatrix} r \left| 1 - \gamma(\gamma\mu + az + \gamma z^2) \right| \\ z - \gamma(-1 + r^2 + z^2) \end{pmatrix}, \tag{16}$$

which is tangent to the identity at the origin and only depends on the parameters (γ, μ). Since *S* is an approximate time-γ map of the vector field $Y_{\gamma,\mu,\omega}$ (11), the locations of the Hopf and heteroclinic bifurcations of *S* are shifted in the parameter space with respect to the corresponding bifurcations of $Y_{\gamma,\mu,\omega}$. These shifts are computed in the next lemma up to order $\mathcal{O}(\gamma)$. We recall that γ is a perturbation parameter, varying in a neighbourhood of 0, while a is a constant belonging to a fixed compact set.

Lemma 2. 1. *For all values of μ and of the constant $a \in \mathbb{C}$, and for γ sufficiently small, the map $\widetilde{S}$ (16) has a unique fixed point $(r_0, z_0)(\gamma, \mu)$, of the form*

$$z_0 = -\frac{\mu}{a_1}\gamma + \mathcal{O}(\gamma^2), \qquad r_0 = 1 + \mathcal{O}(\gamma^2). \tag{17}$$

This fixed point undergoes a Hopf bifurcation at $\mu_{\mathcal{H}}(\gamma) = a_1^2 + \mathcal{O}(\gamma)$, is attracting for $\mu > \mu_{\mathcal{H}}(\gamma)$, and repelling for $\mu < \mu_{\mathcal{H}}(\gamma)$. The estimates in (17) on the order of γ are uniform on compact sets in the constant a and in the parameters (μ, ω).

2. *In a neighbourhood of the origin $(r, z, \gamma) = (0, 0, 0)$, we have*

$$\widetilde{S} = T_{\widetilde{S}}^{\gamma} + \mathcal{O}(\gamma^3) \tag{18}$$

where $T_{\widetilde{S}}^{\gamma}$ is the time-γ map of the planar vector field $T_{\widetilde{S}}$

$$T_{\widetilde{S}}\begin{pmatrix} r \\ z \end{pmatrix} = \begin{pmatrix} -a_1 rz \\ 1 - r^2 - z^2 \end{pmatrix} + \gamma \begin{pmatrix} r\left(-\mu + \dfrac{a_1}{2} - \dfrac{a_1}{2}r^2 - \left(1 + \dfrac{\mathrm{Re}(a^2 + a)}{2}\right)z^2\right) \\ z - (1 + a_1)r^2 z - z^3 \end{pmatrix}. \tag{19}$$

3. *The vector field (19) has a Hopf bifurcation of equilibria for parameters on the curve $\mu_{\mathcal{H}}(\gamma) = a_1^2 + \mathcal{O}(\gamma)$, and it has a heteroclinic connection for*

$$\mu_{\mathcal{H}\mathcal{E}\mathcal{T}} = \frac{a_1}{2} - \frac{b}{3} - \frac{2a_1(1 - a_1) - \frac{bc}{3} - 1}{c + 3} + \mathcal{O}(\gamma),$$

where $b = 1 + \mathrm{Re}(a^2 + a)/2$ and $c = -2/a_1$.

4. *The fixed point $(r_0, z_0)(\gamma, \mu)$ of $\widetilde{S}$ in (17) corresponds to an invariant circle*

$$\mathscr{C} = \left\{ (r_0, z_0, \phi) \ \mid \ \phi \in \mathbb{S}^1 \right\}$$

of the map S (15), having radius r_0 and contained in a horizontal plane $\{z = z_0\}$, where (r_0, z_0) do not depend on ω. The circle $\mathscr{C}$ has the same stability properties as the fixed point (r_0, z_0) of $\widetilde{S}$. The rotation number on $\mathscr{C}$ also depends on ω but the dynamics on $\mathscr{C}$ is always a rigid rotation. Denote $\omega = \omega_0 + \gamma\delta$, where $\omega_0/(2\pi) = 1/5$. For parameter values $(\gamma, \mu, \delta_{1:5}(\gamma, \mu))$, where

$$\delta_{1:5}(\gamma, \mu) = -\frac{a_2 \mu}{a_1}\gamma + \mathcal{O}(\gamma^2), \tag{20}$$

all points on $\mathscr{C}$ have period five for the map S.

5. *For μ bounded away from $\mu_{\mathcal{H}}(\gamma)$, and for γ sufficiently small, the circle $\mathscr{C}$ persists as a normally hyperbolic invariant manifold for the map G (3). The bounds on μ and γ are uniform on compact sets in all other parameters and coefficients of G.*

A fundamental tool for the proof is the Takens normal form vector field [61] of the planar map $\widetilde{S}$ (16), to be denoted by $T_{\widetilde{S}}$ (18).

Remarks 3. 1. As mentioned in item 1 of Lemma 2, all estimates on the order of γ are uniform on compact sets in the constant a and in the parameters (μ, ω). Moreover, in the case of (18) the estimates hold in a sufficiently small neighbourhood of the origin in the variables (w, z).

2. The map S is degenerate, due to the fact that the dynamics on $\mathscr{C}$ is a rigid rotation also for rational rotation numbers. However, description of S provides the 'skeleton' dynamics of the models G and Q. Indeed, the position of the Hopf boundary and of the heteroclinic strip in the two models agrees up to order $\mathcal{O}(\gamma)$ with the values $\mu_{\mathcal{H}}$ and $\mu_{\mathcal{H}\mathcal{E}\mathcal{T}}$ given in Lemma 2. In particular, for $a_1 = -1$ and $\gamma = 0.01$ we have $\mu_{\mathcal{H}} = 1$ and $\mu_{\mathcal{H}\mathcal{E}\mathcal{T}} = 0.35$. Comparison with the numerical results in Section 4 (see [17] and [66, Chap. 4] for more details) suggests that these approximate values are accurate within the error bound, which is of order $\mathcal{O}(\gamma)$.

3. We will show later that the 1:5 resonance gap of G splits linearly in the parameter ε_1 and quadratically in γ around the 1:5 resonant surface $(\gamma, \mu, \delta_{1:5}(\gamma, \mu))$, where $\delta_{1:5}(\gamma, \mu)$ is given in (20). Moreover, the 1:5 bubble splits linearly in ε_1 and quadratically in γ around the curve

$$(\mu_{\mathcal{H}}(\gamma), \delta_{1:5}(\gamma, \mu_{\mathcal{H}}(\gamma))) = \left(a_1^2 + \mathcal{O}(\gamma), -a_1 a_2 \gamma + \mathcal{O}(\gamma^2)\right)$$

in the parameter space (γ, μ, δ). For these parameter values, the circle $\mathscr{C}$ of S consists of period five points and undergoes a Hopf bifurcation.

3.2. Analysis of a vector field approximation

In this section we perform a bifurcation analysis for a vector field approximation of the model G (3). For convenience, the equation of G (3) is here recalled:

$$G : \begin{pmatrix} w \\ z \end{pmatrix} \mapsto \begin{pmatrix} \mathrm{e}^{\mathrm{i}(\omega_0 + \gamma\delta)} w[1 - \gamma(\gamma\mu + az + \gamma z^2)] \\ z + \gamma(1 - |w|^2 - z^2) \end{pmatrix} + \begin{pmatrix} \gamma^3(\varepsilon_1 \overline{w}^4 + \varepsilon_2 z^4) \\ 0 \end{pmatrix}.$$

Throughout the section we assume that ω_0 is fixed at $2\pi/5$. The role of perturbation parameter is played by γ. The parameters (μ, δ) and the remaining coefficients of G are assumed to vary in a fixed compact set. For $\gamma = 0$, the linear part DG at the origin of $\mathbb{R}^3 = \{w, z\}$ is the axial rotation $R_{\omega_0}(w, z) = (e^{i\omega_0}w, z)$. Notice that G is not in Poincaré normal form, due to the presence of the non-resonant term $\varepsilon_2 z^4$. By normal form theory [25,61], there is a transformation such that this term is removed in the new coordinates. We write G in the new coordinates, and restrict to terms of order four in (w, z). This amounts to setting $\varepsilon_2 = 0$ in G, which will be assumed throughout the rest of the section.

Notice that the fifth iterate G^5 is tangent to the identity map at the origin of $\mathbb{R}^3 \times \mathbb{R} = \{w, z, \gamma\}$, while G self is not. This makes G^5 suitable for application of Takens's theorem [61] (also see [66, App. 4.D]). In fact we apply Takens's theorem to a sort of 'fifth root' H of G^5, where H is defined by

$$H(w, z) = \begin{pmatrix} e^{i\gamma\delta}w[1 - \gamma(\gamma\mu + az + \gamma z^2)] + \gamma^3 e^{-i\omega_0}\varepsilon_1\overline{w}^4, \\ z + \gamma(1 - |w|^2 - z^2). \end{pmatrix} \tag{21}$$

The relation between G and H is made precise in the next lemma.

Lemma 3. *For the maps G (3) and H (21) we have*

$$G^5 = H^5 + \mathcal{O}(\gamma^4),$$

where the estimate on the order of γ is uniform on compact sets in the other coefficients and parameters of G and H, and hold in a sufficiently small neighbourhood of the origin in the variables (w, z).

For the map H (21) we compute a vector field approximation T_H such that the time-γ map T_H^γ approximates H up to order four in γ. As in Lemma 3, the estimates on the order of γ given in the next theorem are uniform on compact sets in the remaining coefficients and parameters of the map G and hold in a sufficiently small neighbourhood of the origin in the variables (w, z).

Theorem 4 (*Takens Normal Form Vector Field*). *Consider the vector field T_H given by*

$$T_H = T_{H,0} + \gamma T_{H,1} + \gamma^2 T_{H,2}, \tag{22}$$

where

$$T_{H,0} = \begin{pmatrix} w(i\delta - az) \\ 1 - |w|^2 - z^2 \end{pmatrix}, \tag{23}$$

$$T_{H,1} = \begin{pmatrix} w\left(-\mu + \dfrac{a}{2} - \dfrac{a}{2}|w|^2 - z^2\left(1 + \dfrac{a^2 + a}{2}\right)\right) \\ z - (1 + a_1)|w|^2 z - z^3 \end{pmatrix} \tag{24}$$

$$T_{H,2} = \begin{pmatrix} \varepsilon_1 e^{-i\omega_0}\overline{w}^4 + U_w \\ U_z \end{pmatrix}, \tag{25}$$

and

$$\begin{aligned}
U_w = \ & w\left\{\left(z + ia\frac{\delta}{2}\right)(1 - |w|^2 - z^2) - az\left(\mu + z^2 + \frac{\delta^2}{2} + iaz\delta\right) + i\frac{\delta^3}{3}\right. \\
& + \frac{1}{12}\left[\left((i\delta - az) - a(1 - |w|^2 - z^2)\right)^2 + 2a\left(2(i\delta - az - 2z)(z - (1 + a_1)|w|^2 z - z^3)\right)\right. \\
& \left.\left. + |w|^2 \operatorname{Re}\left[(i\delta - az)^2 - a(1 - |w|^2 - z^2)\right]\right)\right]\right\},
\end{aligned} \tag{26}$$

$$\begin{aligned}
U_z = \ & -|w|^2\left(\mu + z^2 + \frac{\delta^2}{2} - a_2 z\delta\right) + \frac{1}{3}z\left\{(1 - (1 + a_1)|w|^2 - 3z^2)(1 - (1 + a_1)|w|^2 - z^2)\right. \\
& \left. + (1 + a_1)|w|^2 \operatorname{Re}\left[(i\delta - az)^2 - a(1 - |w|^2 - z^2)\right]\right\}.
\end{aligned} \tag{27}$$

Then:

1. *The time-γ map T_H^γ approximates the map H (21) up to order four in γ, i.e., $T_H^\gamma = H + \mathcal{O}(\gamma^4)$.*
2. *The time-5γ map $T_H^{5\gamma}$ approximates the fifth iterate G^5 of (3) up to order four in γ, i.e., $T_H^{5\gamma} = G^5 + \mathcal{O}(\gamma^4)$.*
3. *The vector field T_H is $\mathbb{Z}_5$-equivariant, meaning that it commutes with the axial rotation R_{ω_0}, where $\omega_0/(2\pi) = 1/5$.*
4. *The vector field $T_{H,0} + \gamma T_{H,1}$, given by the terms up to order $\mathcal{O}(\gamma^2)$ of T_H, is axially symmetrical, and its planar reduction coincides with the vector field $T_{\widetilde{S}}$ (19).*

By the last part of Theorem 4 and by Lemma 2, for γ sufficiently small the vector field $T_{H,0} + \gamma T_{H,1}$ has a limit cycle $\mathscr{C}$ contained in a horizontal plane $z = z_0$. For $\mu > \mu_{\mathcal{H}}(\gamma) = a_1^2 + \mathcal{O}(\gamma)$, $\mathscr{C}$ is an attractor, and it is a repellor for $\mu < \mu_{\mathcal{H}}(\gamma)$, where $\mu_{\mathcal{H}}(\gamma)$ is the position of the Hopf bifurcation boundary for T_H, up to order $\mathcal{O}(\gamma^2)$. Moreover, for γ sufficiently small and for μ bounded away from $\mu_{\mathcal{H}}(\gamma)$, $\mathscr{C}$ persists as a normally hyperbolic invariant manifold for the vector field T_H. We are especially interested in the bifurcations taking place near the Hopf bifurcation boundary. The location of the bifurcations of equilibria of T_H near the Hopf boundary is computed in the next theorem,

Theorem 5 (*Tongue and Cone*). *Consider the vector field T_H (22).*

1. *For γ sufficiently small, T_H has ten families $\mathscr{P}_{k,\pm}^5$ of equilibria, $k = 0, \dots, 4$, depending on the parameters (γ, μ, δ''), where*

$$\delta = -\frac{a_2\mu}{a_1}\gamma + \delta''\gamma^2, \qquad \delta'' \in \left(-\frac{|a|}{|a_1|}\varepsilon_1, \frac{|a|}{|a_1|}\varepsilon_1\right).$$

Going back to the original map, the image of a point close to $\mathscr{P}_{k,+}^5$ will be close to $\mathscr{P}_{k+1\bmod5,+}^5$ and similarly for $\mathscr{P}_{k,-}^5$. The cylindrical coordinates $(r_\pm, \phi_{k,\pm}, z_\pm)$ of $\mathscr{P}_{k,\pm}^5$ have the form

$$z_\pm = -\frac{\mu}{a_1}\gamma + z_\pm''\gamma^2 + \mathcal{O}(\gamma^3), \qquad r_\pm = 1 - \frac{\mu^2}{2a_1^2}\gamma^2 + \mathcal{O}(\gamma^3),$$

$$\phi_{k,\pm} = \frac{1}{5}\left(2\pi k - \omega_0 + \arctan\frac{\delta'' - a_2 z_\pm''}{a_1 z_\pm''}\right) + \mathcal{O}(\gamma), \quad k = 0, \dots, 4, \tag{28}$$

where $\phi_{k+1,\pm} - \phi_{k,\pm} = \omega_0$ and

$$z_\pm'' = \frac{a_2\delta'' \pm \sqrt{\Delta}}{|a|^2}, \qquad \Delta = |a|^2\varepsilon_1^2 - a_1^2(\delta'')^2. \tag{29}$$

2. *By decreasing δ (while keeping γ and μ fixed), the ten equilibria are created at five saddle-node bifurcations, occurring simultaneously for $\delta = \delta_{1:5,+}$, and are destroyed (also by five simultaneous saddle-node bifurcations) for $\delta = \delta_{1:5,-}$, where*

$$\delta_{1:5,\pm}(\gamma, \mu) = -\frac{a_2\mu}{a_1}\gamma \pm \frac{|a|}{|a_1|}\varepsilon_1\gamma^2 + \mathcal{O}(\gamma^3). \tag{30}$$

3. *The five equilibria $\mathscr{P}_{k,+}^5$ simultaneously undergo Hopf bifurcations at the surface $\mathcal{H}_+^5$ parameterized by (γ, μ', δ''), where*

$$\mu = a_1^2 + \mu'\gamma + \mathcal{O}(\gamma^2), \qquad \delta = -a_1a_2\gamma + \delta''\gamma^2 + \mathcal{O}(\gamma^3), \tag{31}$$

and the parameters δ'' and μ' depend on each other by the relations

$$\left((2a_1 - 5a_2^2)\mu' - 5a_1a_2\delta''\right)^2 + \left(3a_1a_2\mu' + (3a_1^2 - 2a_1)\delta''\right)^2 = (2a_1 + 2a_1^2 - 5|a|^2)^2\varepsilon_1^2, \tag{32}$$

$$-\delta''a_2(1 + a_1) + (a_1 - a_2^2)\mu' > 0. \tag{33}$$

The five equilibria $\mathscr{P}_{k,-}^5$ simultaneously undergo Hopf bifurcations at the curve $\mathcal{H}_-^5$, defined by (32), where the inequality sign in (33) is reversed.

4. *The cylindrical coordinates of $\mathscr{P}_{k,+}^5$ at the Hopf bifurcations (32) and (33) are*

$$z_\pm = -a_1\gamma + z_\pm''\gamma^2 + \mathcal{O}(\gamma^3), \qquad r_\pm = 1 - \frac{a_1^2}{2}\gamma^2 + \mathcal{O}(\gamma^3),$$

$$\phi_{k,\pm} = \frac{1}{5}\left(2\pi k - \omega_0 + \arctan\frac{\delta'' - a_2 z_\pm''}{\mu' + a_1 z_\pm''}\right) + \mathcal{O}(\gamma), \quad k = 0, \dots, 4,$$

where $\phi_{k+1,\pm} - \phi_{k,\pm} = \omega_0$ and

$$z_\pm'' = \frac{a_2\delta'' - a_1\mu' \pm \sqrt{\Delta'}}{|a|^2}, \qquad \Delta' = |a|^2\varepsilon_1^2 - (a_1\delta'' + a_2\mu')^2. \tag{34}$$

5. *For parameters on the curves $\mathcal{HSN}_\pm^5$ given by $(\gamma, \mu_\pm(\gamma), \delta_\pm(\gamma))$, where*

$$\mu_\pm(\gamma) = a_1^2 \pm \frac{a_2(1 + a_1)}{|a|}\varepsilon_1\gamma + \mathcal{O}(\gamma^2), \qquad \delta_\pm(\gamma) = -a_1a_2\gamma \pm \frac{a_1 - a_2^2}{|a|}\varepsilon_1\gamma^2 + \mathcal{O}(\gamma^3),$$

the equilibria $\mathscr{P}_{k,\pm}^5$ simultaneously undergo five HSN bifurcations. The coordinates of the bifurcating equilibria are

$$z_\pm = -a_1\gamma \pm \frac{a_2}{|a|}\gamma^2 + \mathcal{O}(\gamma^3), \qquad r_\pm = 1 - \frac{a_1^2}{2}\gamma^2 + \mathcal{O}(\gamma^3),$$

$$\phi_{k,\pm} = \frac{1}{5}\left(2\pi k - \omega_0 + \arctan\frac{a_1}{a_2}\right) + \mathcal{O}(\gamma), \quad k = 0, \ldots, 4,$$

i.e., $e^{i\phi_{k,\pm}}$ *are the fifth roots of* $\frac{i\bar{a}}{|a|}e^{-i\omega_0}$.

6. *Suppose that the coefficients of* H *are fixed at* $\varepsilon_1 = \varepsilon_2 = 1$, $a_1 = -1$ *and* $a_2 = 1/\sqrt{2}$. *Then* $\mathcal{HSN}^5_\pm$ *belong to the same unfolding class of Hopf saddle-node bifurcations. To be precise, for* $k = 0, \ldots, 4$ *denote by*

$$Y_{\beta,k,\pm}(w,z) = \begin{pmatrix} (-\beta_{2,k,\pm} + i\omega_{5,\pm})w - a_{5,\pm}wz - wz^2 \\ -\beta_{1,k,\pm} - s_{5,\pm}|w|^2 - z^2 \end{pmatrix} \tag{35}$$

the truncated normal form of T_H *as a HSN vector field (as in* [48, *Lemma 8.11*]), *after translation of* T_H *into the singularity* $\mathscr{P}^5_{k,\pm}$. *Then the coefficients* $\mathrm{Re}(a_{5,\pm})$ *and* $s_{5,\pm}$ *in* (35) *are*

$$\mathrm{Re}(a_{5,\pm}) = -1 + \mathcal{O}(\gamma), \qquad s_{5,\pm} = \mathrm{sign}(\gamma),$$

and a reversal of time is introduced by the transformation bringing T_H *into* (35).

In the parameter space (γ, μ, δ), the surfaces $\mathcal{SN}^5_\pm$ delimit a tongue whose width is quadratic in γ, and shrinks to a line for $\gamma \to 0$. The Hopf bifurcations $\mathcal{H}^5_\pm$ form a cone-like surface contained in the interior of the three-dimensional tongue, see the illustration in Fig. 4 (top left panel). The vertex of the cone is the point $(\gamma, \mu, \delta) = (0, 1, 0)$, where the derivative DT_H at the equilibrium $(w, z) = (1, 0)$ is equal to zero. This is a special case of the three-dimensional nilpotent singularity studied in [29,30]. Also see [28] for a detailed study of the HSN for vector fields. Near the 1:5 bubble, the bifurcation diagram of T_H is organized by the two Hopf-saddle-node bifurcations of equilibria $\mathcal{HSN}^5_\pm$, proved to occur in Theorem 5. At such points, there are five degenerate equilibria on $\mathscr{C}$ which undergo a Hopf and a saddle-node bifurcation simultaneously. The intersection of the bifurcation surfaces $\mathcal{SN}^5_\pm$ (30) and $\mathcal{H}^5_\pm$ (31) with the plane $\gamma = 0.01$ is plotted in Fig. 4 (top right panel).

The dynamic analogies between the vector field T_H (22) and the map G (3) are a corollary of Theorem 5. Indeed, the fifth iterate G^5 is a perturbation of the time-5γ map $T_H^{5\gamma}$. Therefore, by application of perturbation theory the bifurcations $\mathcal{SN}^5_\pm$, $\mathcal{H}^5_\pm$, and $\mathcal{HSN}^5_\pm$ in Theorem 5 persist for the map G^5. By perturbation theory we mean the implicit function theorem, the theory of persistence of normally hyperbolic invariant manifolds [33,40], the theory of persistence of nondegenerate bifurcations [3,37,48, 53,55,56], including quasi-periodic bifurcations [9,10,22,23], and KAM theory [2,3,9,10].

Indeed, there is excellent agreement between the results obtained in Theorem 5 for the vector field T_H (22) (Fig. 4, top row) and the numerical results obtained for model map G (3) (Fig. 4, bottom row). The latter results are discussed in some detail next.

4. A preliminary numerical investigation near the 1:5 resonance 'bubble'

The analytical study in Section 3 is here complemented by a sketch of the numerical results which we have obtained for model map G (3). Referring to Section 2.3, we recall that our main interest is the interaction of the 1:5 resonance gap with the Hopf bifurcation boundary See [6,20,22–24,49,50,64,68,69] for similar studies inside resonance bubbles. In the next subsection, we discuss a partial bifurcation diagram of periodic points, invariant circles and two tori. Then in Section 4.2 a few scenarios are discussed concerning some of the configurations of attractors, repellors and saddles that have been observed in phase space for the model map G. A full account of these numerical results will be given in [17].

4.1. Lyapunov diagram and bifurcation diagram

A first impression of the richness of the bifurcation diagram near the 1:5 resonance bubble on the Hopf boundary $\mathcal{H}$ is given by the 'Lyapunov diagram' [59,66] in Fig. 4, bottom left panel. The diagram has been computed with the same values of the coefficients of G as in part 6 of Theorem 5 and with γ fixed at 0.1. This Lyapunov diagram is a plot of the (μ, δ)-parameter plane, where each colour corresponds to one type of attractor, classified on the basis of the Lyapunov exponents

$$\ell_1 \geq \ell_2 \geq \ell_3,$$

according to the colour code in Table 1. The algorithm used to scan the parameter plane runs as follows: in a first naive set-up we scan the (μ, δ)-parameter plane along horizontal lines $\delta = const$ from right to left. Fixing δ, say at 0.1, we choose a value of μ, say $\mu = 1.5$. Then a fixed number of iterates of the map G is computed. Whenever the orbit has converged to an attractor, *i.e.*, when it has not left a prescribed neighbourhood of the origin after a large number of iterates (say, 10^6), the three Lyapunov exponents ℓ_1, ℓ_2 and ℓ_3 are computed. Next we decrease μ by a small step and the procedure is restarted, until μ reaches the value 0. Regarding the initial conditions we do the following. Starting with an 'arbitrary' choice, in all following steps we take the final state of the previous number of iterates as initial condition. This whole procedure is repeated for many values of δ.
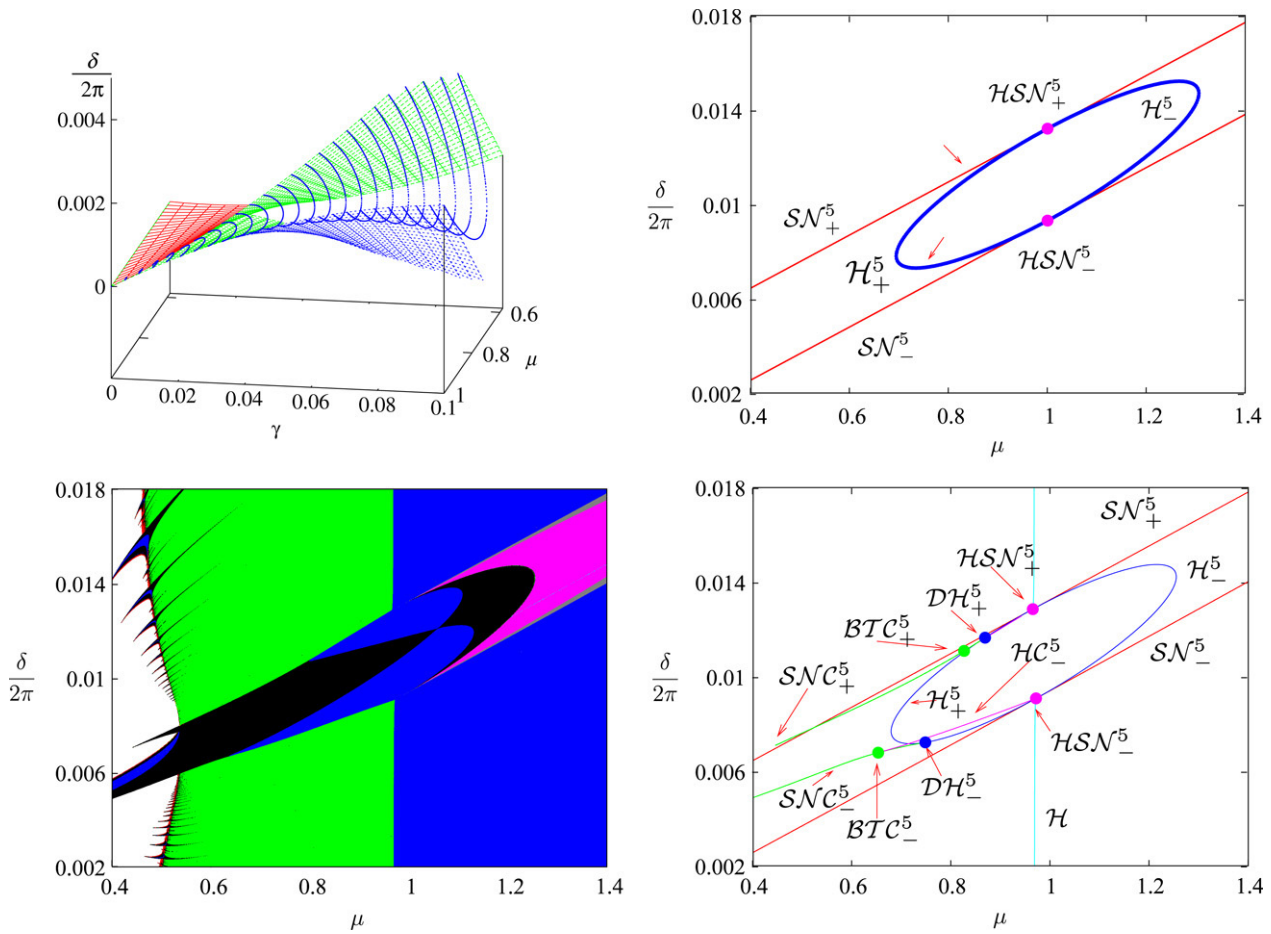
Fig. 4. Top, left: the 1:5 resonance tongue bounded by the saddle-node bifurcation surfaces $\mathcal{SN}^5_\pm$ contains the cone-like Hopf bifurcation set $\mathcal{H}^5_\pm$ according to Theorem 5. Only a part of the surfaces is displayed, and the graph has been deformed for better visibility. Top, right: intersection of the bifurcation surfaces in the left picture with the plane $\gamma = 0.01$ yields a resonance gap bounded by two curves $\mathcal{SN}^5_\pm$ of saddle-node bifurcations, containing an ellipse of Hopf bifurcations of equilibria of the vector field T_H (22). Bottom, left: Lyapunov diagram of map G near the intersection of the 1:5 resonance gap with the Hopf boundary $\mathcal{H}$. Right: numerical bifurcation diagram of the map G near $\mathcal{H}$. The notation is explained in the text. Same parameter window as in the bottom-left and top-right panels. The coefficients of vector field T_H (22) and of model map G (3), used to plot each of the panels, have the same values as in point 6 of Theorem 5.

Table 1
Legend of the colour coding for Fig. 4 bottom left panel: the attractors are classified by means of the Lyapunov exponents (ℓ_1, ℓ_2, ℓ_3) (For the interpretation of the references to colour in Fig. 4, the reader is referred to the web version of this article)

Colour	Lyapunov exponents	Attractor type
Red	$\ell_1 > 0 = \ell_2 > \ell_3$	Strange attractor
Yellow	$\ell_1 > 0 > \ell_2 > \ell_3$	Strange attractor
Blue	$\ell_1 = 0 > \ell_2 = \ell_3$	Invariant circle of focus type
Green	$\ell_1 = \ell_2 = 0 > \ell_3$	Invariant two-torus
Black	$\ell_1 = 0 > \ell_2 > \ell_3$	Invariant circle of node type
Grey	$0 > \ell_1 > \ell_2 = \ell_3$	Periodic point of focus type
Fuchsia	$0 > \ell_1 = \ell_2 \geq \ell_3$	Periodic point of focus type
Pale blue	$0 > \ell_1 > \ell_2 > \ell_3$	Periodic point of node type
White		No attractor detected

Note that in this setup we fail to detect invariant manifolds which are of saddle type or repelling. Moreover, the method cannot detect coexistence of attractors, since we continue one attractor until there is a qualitative change in the ℓ_j, $j = 1, 2, 3$, in which case there may be a jump. This entails a form of hysteresis and a different Lyapunov diagram is formed, e.g. when the $(\mu, \delta/(2\pi))$-plane is scanned in other directions. For this reason we actually use a more sophisticated way to scan the $(\mu, \delta/(2\pi))$-plane, using other scan directions as well. This allows to detect more families of attractors: the curved peaks at the left hand side of the Lyapunov diagram are not detected by the 'naive' algorithm.

From the Lyapunov diagram, we conclude that the generic expectations discussed in Section 2.3 are largely met by model G (3). For large positive values of μ there exists a circle attractor $\mathscr{C}$ (blue domain at the right part of the Fig. 4, bottom left panel), that undergoes a quasi-periodic Hopf bifurcation approximately at the vertical line $\mu = 0.98$. The latter corresponds to the intersection $\mathcal{H} \cap \{\gamma = 0.1\}$, where $\mathcal{H}$ is the 'Cantor-surface' in Fig. 3 right. Roughly speaking, as μ decreases, the circle $\mathscr{C}$ loses its stability and turns into a repellor, whereby an attracting invariant two-torus $\mathscr{T}_-$ branches off (green region). The 1:5 resonance gap of the circle $\mathscr{C}$ is evidenced by the fuchsia strip at the right of the Lyapunov diagram. In the blue regions outside this gap, the dynamics on $\mathscr{C}$ is quasi-periodic and normal-internal resonances are also forbidden [7,9,10,26].

A partial bifurcation diagram of periodic points and invariant circles is given in Fig. 4 right, which involves:

1. Two branches $\mathcal{H}^5_\pm$ of Hopf bifurcations of period five points, that form a closed curve. We refer to the union of $\mathcal{H}^5_\pm$ as the 'Hopf ellipse'.
2. Two lines $\mathcal{SN}^5_\pm$ of saddle-node bifurcations of period five points. These two lines bound a strip in parameter plane which we refer to as the '1:5 gap' (also see the end of Section 2.3).
3. Two points $\mathcal{HSN}^5_\pm$ of Hopf saddle-node bifurcations of period five points, that split the Hopf ellipse into $\mathcal{H}^5_+$ and $\mathcal{H}^5_-$. The curve $\mathcal{SN}^5_+$ and $\mathcal{SN}^5_-$ are tangent to the Hopf ellipse at $\mathcal{HSN}^5_+$ and $\mathcal{HSN}^5_-$, respectively.
4. Two degenerate Hopf bifurcations $\mathcal{DH}^5_\pm$ of period five points, taking place along $\mathcal{H}^5_+$.
5. Two 'curves' $\mathcal{HC}^5_\pm$ of quasi-periodic Hopf bifurcations of a period five invariant circle; $\mathcal{HC}^5_+$ is not visible in Fig. 4 right, since it is too close to $\mathcal{H}^5_\pm$.
6. Two 'curves' $\mathcal{SNC}^5_\pm$ of quasi-periodic saddle-node bifurcations of a period five invariant circle.
7. Two 'curves' $\mathcal{SNT}_\pm$ of quasi-periodic saddle-node bifurcations of an invariant two-torus (both are not displayed in Fig. 4 right, since they are very close to $\mathcal{HC}^5_\pm$);
8. Two 'points' $\mathcal{BTC}^5_\pm$ where Bogdanov-Takens bifurcations of period five invariant circles take place (please, see below for the definition).

Existence of the curves $\mathcal{H}^5_\pm$ and $\mathcal{SN}^5_\pm$, as well as of the points $\mathcal{HSN}^5_\pm$, has been proved by analytical means in Theorem 5. The quasi-periodic bifurcations of invariant circles are computed by monitoring their normal behaviour: for this purpose, the algorithm described in [43] has been used (called the "large matrix method" in [38]), whereas the computation of quasi-periodic invariant circles is performed by Fourier analysis [31,32]. We refer the reader to [35,38,39,51,58] and references therein for other methods and examples.

Remark 4. For quasi-periodic bifurcations, the word 'curves' is enclosed in quotes since the corresponding parameter sets are not smooth submanifolds of the parameter plane: they are frayed Cantorlike bifurcation boundaries interspersed of resonance bubbles. In fact, the theoretical expectation for $\mathcal{SNC}^5_\pm$ and $\mathcal{HC}^5_\pm$ is *exactly the same* as for the Hopf boundary $\mathcal{H} \cap \{\gamma = 0.1\}$ self, as discussed in Section 2.3: we expect most of the dynamic complexity described there also to occur near all the secondary quasi-periodic bifurcation 'curves' in Fig. 4 right, in a sort of cascade of subordinate quasi-periodic bifurcations. Indeed, resonance gaps are often detected along the numerical continuation of the above 'curves'. However, since most of the gaps are tiny, the continuation algorithm is able to skip over them.

A description of the bifurcation diagram follows, focusing on the lower branches of the 'curves', that is $\mathcal{HC}^5_-$, $\mathcal{SNC}^5_-$, and $\mathcal{SNT}_-$. A completely symmetrical situation seems to hold for the upper branches $\mathcal{HC}^5_+$ and $\mathcal{SNT}_+$. The quasi-periodic saddle-node 'curve' $\mathcal{SNC}^5_-$ joins the points $\mathcal{BTC}^5_-$ and $\mathcal{DH}^5_-$. The latter point is a degenerate Hopf bifurcation belonging to the Hopf ellipse, where $\mathcal{SNC}^5_-$ 'meets tangentially' the left branch $\mathcal{H}^5_+$ and there it terminates (again, quotes are used since $\mathcal{SNC}^5_-$ is a Cantor set). This is the situation described by Chenciner [22–24]. The quasi-periodic Hopf 'curve' $\mathcal{HC}^5_-$ joins the points $\mathcal{HSN}^5_-$ and $\mathcal{BTC}^5_-$. At the latter 'point' the 'curve' $\mathcal{HC}^5_-$ 'meets tangentially' $\mathcal{SNC}^5_-$. Here, both $\mathcal{SNC}^5_-$ and $\mathcal{HC}^5_-$ are frayed Cantor-like boundaries and the definition of tangency requires the usage of Whitney derivatives [9]. The ubiquitous occurrence of resonances makes it hard to decide whether the tangency point $\mathcal{BTC}^5_-$ between the two Cantor sets belongs to both of them or if it falls inside one of the resonance bubbles. To the best knowledge of the authors, this codimension two point has not yet been studied. Based on analogy with the Bogdanov-Takens bifurcation for fixed points [12,13,60] (which is also called 1:1 resonance [48]) we guess that the bifurcation diagram near $\mathcal{BTC}^5_-$ also involves bifurcations of global (homoclinic) type, but we have not further pursued this research.

The 'curve' $\mathcal{SNT}^5_-$ of quasi-periodic saddle-node bifurcations of invariant tori begins at the point $\mathcal{HSN}^5_-$ and terminates somewhere near the Bogdanov-Takens 'point' $\mathcal{BTC}^5_-$ Furthermore, there exists a narrow parameter region $\mathcal{HET}^5_-$, located very near $\mathcal{SNT}_-$, where both transversal heteroclinic intersections and heteroclinic tangencies of two period five points of saddle-focus type occur. At the present stage of the investigation, an approximation to the 'curve' $\mathcal{SNT}^5_-$ has been obtained by just looking at attractors and repellors of model map G Eq. (3). Fourier methods [31,32] might be used to compute it more accurately. However, we observe that for a diffeomorphism at least a three-dimensional parameter space is necessary to find a smooth submanifold parameterizing a Diophantine family of invariant two-dimensional tori: as prescribed by dissipative KAM theory [7,9,10,26],
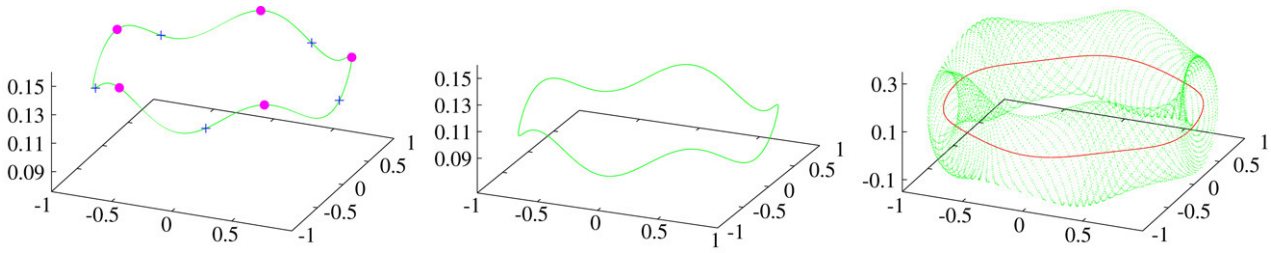
Fig. 5. Left: the attracting invariant circle $\mathscr{C}$ of model map G (3) for $(\delta/(2\pi), \mu) = (0.0167, 1.4)$ is phase-locked: $\mathscr{C} = W^u(P_+^5) \cup P_-^5$, where P_+^5 is a period five orbit of saddle-focus type (displayed as blue crosses), $W^u(P_+^5)$ is plotted in green and P_-^5 is an attracting period five orbit of node-focus type (small circles, fuchsia). Middle: the invariant circle $\mathscr{C}$ is an attractor and 'looks' quasi-periodic (densely filled by the orbit), $(\delta/(2\pi), \mu) = (0.0167, 1)$. Right: the circle $\mathscr{C}$ (red) coexists with the invariant two torus $\mathscr{T}$ (green), both 'look' quasi-periodic, $(\delta/(2\pi), \mu) = (0.0167, 0.94)$. (For interpretation of the references to colour in this figure legend, the reader is referred to the web version of this article.)

parameter sets where the frequency vector of the invariant two-torus is fixed to a constant value are *discrete* (zero-dimensional) in the (δ, μ)-plane. So even if one of the two frequencies is fixed to a Diophantine value, resonances of the other frequency (or of the whole frequency vector) are unavoidable as parameter vary smoothly in the (δ, μ)-plane. This everywhere dense network of resonances is the so-called *Arnol'd web*, further described in [16,17] and [66, Chap 4]. The unavoidable occurrence of resonances is likely to cause numerical problems in the continuation algorithm for the two-torus: high order of the spectral discretization is required to obtain convergence, especially for the computation of the normal behaviour.

Many bifurcation curves in Fig. 4 (bottom right panel) have a counterpart in the Lyapunov diagram (bottom left panel). For example, $\mathcal{SNC}_+^5$ and $\mathcal{SNC}_-^5$ are the top and bottom boundary, respectively, between the black and green regions at the left of the Hopf boundary $\mathcal{H} \cap \{\gamma = 0.1\}$ in the Lyapunov diagram. Moreover, the 'curve' $\mathcal{SNT}_-$ is the lower boundary between green and blue regions, at the left of the Hopf boundary. However, we emphasize that the transition from black to blue in the Lyapunov diagram is not a bifurcation: it is just a change of stability type of an invariant circle, from node to focus). It turns out that quite a few invariant manifolds are involved:

1. two families of period five points $P_\pm^5$;
2. an invariant circle $\mathscr{C}$;
3. two families of period five invariant circles $\mathscr{C}_\pm^5$;
4. an attracting and a repelling invariant two-torus ($\mathscr{T}_-$ and $\mathscr{T}_+$, respectively);
5. a repelling period five invariant two-torus $\mathscr{T}_+^5$.

Next, we illustrate a few scenarios in phase space, involving some of the invariant objects listed above.

4.2. Rich dynamics

Here we describe a few configurations in phase space of the invariant objects (attractors, repellors, saddles) of model map G (3). A full, detailed description of the dynamics for parameters belonging to the various regions identified in Fig. 4 would be out of the scope of the present paper: we refer the interested reader to [17].

In Fig. 5, left panel, the circle $\mathscr{C}$ is plotted for parameter values inside the 1:5 resonance gap (that is, inside the fuchsia strip in Fig. 4 bottom left panel): the circle is phase locked, that is $\mathscr{C} = W^u(P_+^5) \cup P_-^5$, where P_-^5 is an attracting period five orbit of node-focus type and P_+^5 is a period five orbit of saddle-focus type. In other words, the dynamics on $\mathscr{C}$ is of Kupka–Smale type. However, a check of the eigenvalues at P_-^5 indicates that $\mathscr{C}$ is not normally hyperbolic: the eigenvalue in the 'node' direction (tangential to $\mathscr{C}$) is real and the corresponding Lyapunov exponent is $\ell_1 = -0.0273$, while the Lyapunov exponents corresponding to the complex conjugate eigenvalues (in the 'focus' direction, normal to $\mathscr{C}$) are $\ell_2 = \ell_3 = -0.0093$. Therefore, normal contraction is weaker than tangential contraction at the attracting node P_-^5. This indicates that near the Hopf bifurcation boundary in certain regions the circle might persist despite the loss of normal hyperbolicity. When decreasing the parameter μ, the circle exits the 1:5 gap: for example, for $\mu = 1$ the orbits of G appears to densely fill $\mathscr{C}$ (Fig. 5, centre panel). As μ crosses the Hopf boundary outside the 1:5 bubble, a two-torus attractor branches off and $\mathscr{C}$ turns into a repellor (Fig. 5, right panel).

The bifurcation routes are more involved inside the 1:5 bubble. Start again at the parameter values of Fig. 5, left panel: when decreasing μ and δ in such a way as to cross the curve $\mathcal{H}_-^5$ (see Fig. 4, bottom right panel), the period five attractor P_-^5 undergoes a Hopf bifurcation, and a period five invariant circle $\mathscr{C}_-^5$ branches off. At this moment, the period five circle attractor $\mathscr{C}_-^5$ coexists with two period five points, both of saddle focus type: P_-^5, marked as a cross, which has a one-dimensional stable manifold; and P_+^5, marked as a small solid circle, which has a one-dimensional unstable manifold. Moreover, the phase-locked circle $\mathscr{C}$ no longer exists. The configuration in phase space is illustrated in Fig. 6, left panel.

By further decreasing μ and δ in such a way as to go 'on the other side of the bubble', across the curve $\mathcal{H}_+^5$ (again, see Fig. 4, bottom right panel), the period five saddle point P_+^5 undergoes a Hopf bifurcation and turns into a repellor, while a period five
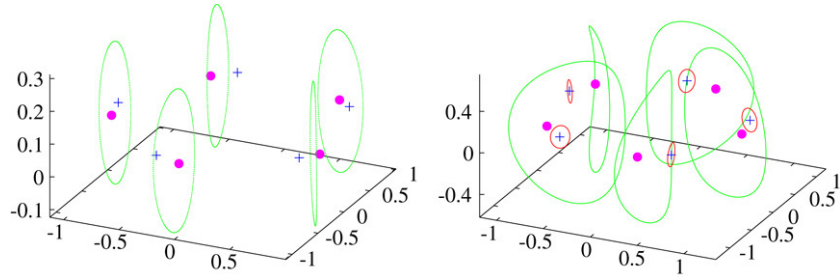
Fig. 6. Left: the period five attracting invariant circle $\mathscr{C}^5_-$ (in green) of model map G (3) for $(\mu, \delta/(2\pi)) = (1, 0.0097)$ coexists with two period five points of saddle-focus type: P^5_+ (displayed as blue crosses), which has a one-dimensional unstable manifold, and P^5_- (small circles, fuchsia), which has a one-dimensional stable manifold. Right: at $(\mu, \delta/(2\pi)) = (0.74675, 0.0097607)$ the period five attracting invariant circle $\mathscr{C}^5_-$ (green) coexists with a period five invariant circle $\mathscr{C}^5_+$ of saddle type (red) and with two period five points: P^5_+ (blue crosses), which is a repelling node focus, and P^5_- (small circles, fuchsia), which is a saddle focus with a one-dimensional stable manifold. (For interpretation of the references to colour in this figure legend, the reader is referred to the web version of this article.)
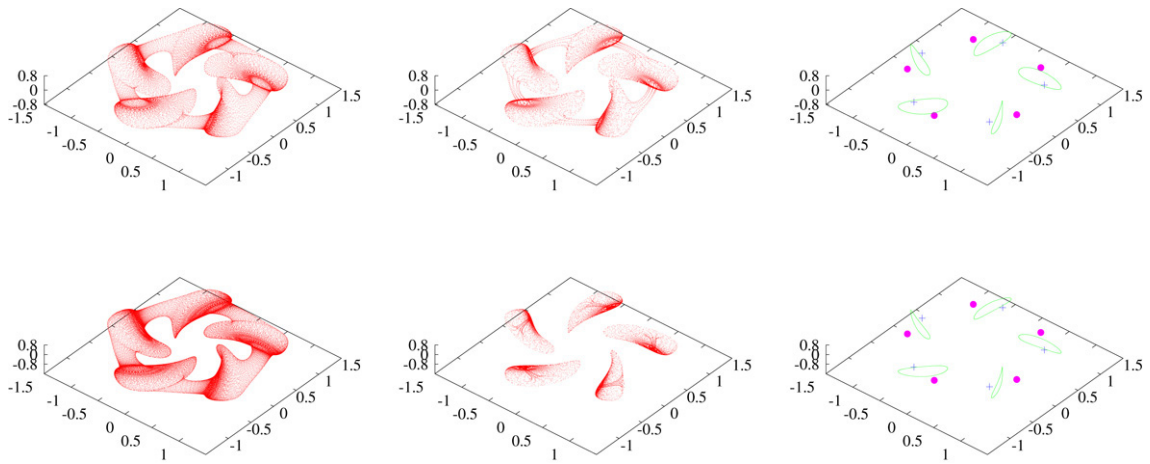

Fig. 7. Top row: a two-torus attractor (left panel) coexists with a two-torus repellor (middle), with a period five circle attractor $\mathscr{C}^5_-$ and with two period five points having different stability index (right panel), P^5_+ (displayed as blue crosses) which has a one-dimensional unstable manifold, and P^5_- (small circles, fuchsia) with a one-dimensional stable manifold. Parameter values are fixed at $(\mu, \delta/(2\pi)) = (0.72, 0.0072265)$. Bottom row: for $(\mu, \delta/(2\pi)) = (0.72, 0.00722673)$, the two-torus attractor, the period five circle and the two period five points persist and are almost unchanged (this explains the similarity between top and bottom panels at the right and at the left). The two-torus repellor has been destroyed (probably, by a heteroclinic bifurcation) and a period five two-torus repellor has shown up in its place (middle panel). (For interpretation of the references to colour in this figure legend, the reader is referred to the web version of this article.)

invariant circle $\mathscr{C}^5_+$ branches off. In this configuration (Fig. 6, right panel), two period five invariant circles $\mathscr{C}^5_+$ (of saddle type) and $\mathscr{C}^5_-$ (attractor) coexist with two period five points, P^5_+ (repellor) and P^5_- (saddle focus). Moreover, the circle $\mathscr{C}$ reappears and is phase locked: $\mathscr{C} = W^u(P^5_-) \cup P^5_+$, but for these parameter values it is repelling (for better visibility, $W^u(P^5_-)$ is not shown in the picture). Simultaneously, a phase-locked two-torus attractor $\mathscr{T}$ exists: it is formed by the unstable manifold of the saddle-like circle $\mathscr{C}^5_+$ (not shown in the picture), that is, $\mathscr{T} = W^u(\mathscr{C}^5_+) \cup \mathscr{C}^5_-$. For parameter values belonging to the 'curves' $\mathcal{SNC}^5_\pm$ (compare Fig. 4 bottom right panel), the two period five invariant circles $\mathscr{C}^5_+$ and $\mathscr{C}^5_-$ collide with each other and disappear through a quasi-periodic saddle-node bifurcation. Depending on the parameter range, the two-torus might reappear: this happens on the transition from black to green in the Lyapunov diagram (Fig. 4 bottom left panel). This also means that the quasi-periodic saddle-node bifurcation takes place *inside* the surface of the two-torus.

The presence of additional bifurcations of invariant circles and two-tori leads to rather pictorial configurations in phase space. A pair of two-tori is created through a quasi-periodic saddle-node bifurcation taking place at 'curve' $\mathcal{SNT}_\pm$ in parameter plane (see Fig. 4, bottom right panel). As a consequence, for certain parameter values we have a torus attractor coexisting with a torus repellor and the latter is contained inside the volume bounded by the former. Also, the two-torus repellor bounds a volume containing the period five invariant circle $\mathscr{C}^5_-$, which is an attractor, and the two period five points $P^5_\pm$, which are saddles with different stability indexes. This configuration is illustrated in Fig. 7, top row. For nearby parameter values, the two-torus repellor is destroyed and a period five torus repellor appears in its place, surrounding the period five circle $\mathscr{C}^5_-$. See Fig. 7 bottom row. The mechanism leading to the destruction of the two-torus repellor most probably involves a heteroclinic bifurcation of $P^5_\pm$ and leads to the formation of a strange repellor; the latter scenario is still under investigation. Lastly, at the 'curve' $\mathcal{HC}^5_\pm$ (see Fig. 4, bottom right panel)the period five torus repellor merges with the period five circle $\mathscr{C}^5_-$ through a quasi-periodic Hopf bifurcation, whereby $\mathscr{C}^5_-$ turns into a repellor.

5. Conclusions

As we have shown, the Hopf-saddle-node (HSN) bifurcation for fixed points of diffeomorphisms displays a large variety of dynamical phenomena. In this paper we have studied the model map G given by (3). This is constructed by perturbing the time-1 map of the flow of the axially symmetrical vector field (6), which is a truncated normal form for the HSN bifurcation of vector fields. The model map G aims at describing the dynamics of a large class of HSN diffeomorphisms in the vicinity of a 1:5 resonance 'bubble' for a quasi-periodic Hopf bifurcation. The results in Section 3 provide estimates for the position of:

1. a 1:5 resonance gap of an invariant circle $\mathscr{C}$, bounded by two saddle-node bifurcations $\mathcal{SN}^5_\pm$ (30) of period five points;
2. a cone-like surface $\mathcal{H}^5_\pm$ (31) of Hopf bifurcations of period five points;
3. two HSN bifurcations of period five points.

We recall that many features of the structure of the 1:5 bubble analysed here are found in resonance bubbles of different orders, found in model maps of the Hopf–flip and Hopf–Hopf bifurcations of fixed points [49,50].

The results in Section 4 indicate that many more bifurcations take place in the neighbourhood of this 1:5 'bubble'. We plan to extend the analysis of the Takens normal form vector field, initiated in Theorem 5, to prove the occurrence of such bifurcations. In this respect, we conjecture that the bifurcations $\mathcal{SN}^5_\pm$ take place *on the invariant circle $\mathscr{C}$*. In the terminology of [48], and modulo the 1:5 symmetry, these are called saddle-node homoclinic bifurcation. Near these bifurcations, the circle $\mathscr{C}$ is normally hyperbolic and it is phase-locked: it is formed by the unstable manifolds of one of the two families of equilibria $\mathscr{P}^5_{k,\pm}$. We also conjecture that the bifurcations $\mathcal{HSN}^5_\pm$ of T_H take place on the circle $\mathscr{C}$, yielding a Hopf saddle-node homoclinic bifurcation (in the terminology of [48]) or Hopf saddle-node with global reinjection in the terminology of [45]. A planar model vector field is considered in the latter paper. There are many analogies between the bifurcation diagrams of T_H (Fig. 4, top panels) and of this planar vector field: in fact, several bifurcations of the latter correspond to the bifurcations of invariant circles and invariant tori of the model G (3) discussed in Section 4. A three-dimensional model vector field for the Hopf saddle-node bifurcation with global reinjection has been studied in [46]: homoclinic orbits were found, displaying multiple excursion out of and back into a neighbourhood of the Hopf saddle-node equilibrium point. The relation between the vector fields T_H Eq. (22) and those considered in [45,46], as well as the completion of the bifurcation diagram of T_H in Fig. 4 top panels, are still under investigation by the authors. Another point of interest to us is whether there exists a relation between the conelike structure found for the HSN bifurcation and the nilpotent singularity analysed in [29,30].

Beyond the bifurcation structure of the 1:5 bubble, other points of interest, introduced in Section 2.3, are:

1. The Arnol'd web of resonances in parameter plane, induced by the two-torus dynamics;
2. The two-torus breakdown and the formation of strange attractors in the region $\mathcal{HET}$ of heteroclinic intersections of the polar saddles.

More detailed investigations of these two issues are given in [16,17], respectively.

Acknowledgements

Appendix A. Normal form lemmas

In Appendix A.1 we describe the normalization steps which bring a generic HSN-family of vector field to the form (7), then in Appendix A.2, we prove a version of Takens's theorem [61] which is then used in Appendix B for the proof of Theorem 1.

A.1. Normal form for HSN-families of maps

The purpose of this section is to present an analogue of the results in [48, Sec. 8.5.1] for a given HSN-family of diffeomorphisms F, depending on the multi-parameter $\alpha = (\alpha_1, \ldots, \alpha_k)$. Notice that fewer simplifications are possible for a diffeomorphism than for vector fields, since we cannot scale time. Moreover, in this case three parameters are needed for the Linear Centralizer Unfolding of $DF(0, 0)$, hence we set $k = 3$. Assume the linear part of F is in Jordan normal form:

$$F_\alpha(w, z) = \begin{pmatrix} f_{000} + \lambda(\alpha)w + \sum_{j+k+h \geq 2} f_{jkh}(\alpha)\, w^j \overline{w}^k z^h \\ g_{000} + \nu(\alpha)z + \sum_{j+k+h \geq 2} g_{jkh}(\alpha)\, w^j \overline{w}^k z^h \end{pmatrix}, \tag{36}$$

where $\nu(0) = 1$ and $\lambda(0) = \lambda_0$, while $f_{000}(0) = g_{000}(0) = 0$.

Lemma 6. *Let F be an HSN-family of diffeomorphisms as in* (36), *depending on the multi-parameter $\alpha \in \mathbb{R}^3$, with* spec $DF_0(0) = \{\lambda_0, \overline{\lambda}_0, 1\} \subset \mathbb{S}^1$. *Suppose F satisfies the open and dense condition*

$$g_{002}(0) \neq 0, \quad g_{110}(0) \neq 0. \tag{37}$$

Also assume that the derivative of the map

$$\alpha \mapsto (g_{000}(\alpha), \lambda(\alpha)) \tag{38}$$

is surjective at $\alpha = 0$. Then there exist a smooth parameter-dependent transformation and a reparameterization $\beta = (\beta_1, \beta_2, \beta_3)(\alpha)$, with $\beta_j \in \mathbb{R}$, such that in the new coordinates and parameters the diffeomorphism (36) *reads*

$$\begin{pmatrix} w \\ z \end{pmatrix} \mapsto \begin{pmatrix} (1 + \beta_2)\mathrm{e}^{\mathrm{i}\beta_3}\lambda_0 w + awz + bwz^2 \\ \beta_1 + z + sw\overline{w} + z^2 + cz^3 \end{pmatrix} + \mathcal{O}(\|w, z\|^4). \tag{39}$$

Here the coefficients $a(\beta)$ and $b(\beta)$ are complex, while $c(\beta)$ is real and $s = \pm 1$.

The proof is divided in two parts. First we consider the normalizing procedure for $\alpha = 0$. This is achieved by two transformations performed independently. For small α the conclusion follows from the implicit function theorem, but the two transformations have to be performed simultaneously. Finally, a parameter-dependent scaling of the variables is applied. We begin by setting $\alpha = 0$.

Step 1. Poincaré normal form.

By general theory [25,61], for $\alpha = 0$ there exists a change of coordinates in $\mathbb{R}^3$ which is tangent to the identity at the origin, and such that in the new coordinates only resonant monomial appear in the expansion of F. For $n \geq 2$ integer, a monomial P of the form

$$P(w, z) = w^{n_1}\overline{w}^{n_2}z^{n_3}$$

is called *resonant* if it commutes with the semisimple part S of $DF_0(0)$. Because of (2), in suitable coordinates $(\hat{w}, \hat{z})$ the 3-jet of any HSN-family at $\alpha = 0$ is axially symmetrical

$$\begin{pmatrix} \lambda_0\hat{w} + \hat{f}_{101}\hat{w}\hat{z} + \hat{f}_{210}\hat{w}^2\overline{\hat{w}} + \hat{f}_{102}\hat{w}\hat{z}^2 \\ \hat{z} + \hat{g}_{110}\hat{w}\overline{\hat{w}} + \hat{g}_{002}\hat{z}^2 + \hat{g}_{111}\hat{w}\overline{\hat{w}}\hat{z} + \hat{g}_{003}\hat{z}^3 \end{pmatrix} + \mathcal{O}\left(\|\hat{w}, \hat{z}\|^4\right). \tag{40}$$

Step 2. Second order Poincaré normalization (hypernormalization) [48].

Denote by $\widehat{F}$ the map in (40). By a transformation of the form

$$(\hat{w}, \hat{z}) = C(\hat{\hat{w}}, \hat{\hat{z}}) = (\hat{\hat{w}} + b_1\hat{\hat{w}}\hat{\hat{z}}, \ \hat{\hat{z}} + b_2\hat{\hat{z}}^2),$$

the cubic terms $\hat{w}^2\overline{\hat{w}}$ and $\hat{w}\overline{\hat{w}}\hat{z}$ in (40) can be eliminated, yielding the map $\widehat{\widehat{F}}$:

$$\widehat{\widehat{F}}(\hat{\hat{w}}, \hat{\hat{z}}) = \begin{pmatrix} \lambda_0\hat{\hat{w}} + \hat{\hat{f}}_{101}\hat{\hat{w}}\hat{\hat{z}} + \hat{\hat{f}}_{102}\hat{\hat{w}}\hat{\hat{z}}^2 \\ \hat{\hat{z}} + \hat{\hat{g}}_{110}\hat{\hat{w}}\overline{\hat{\hat{w}}} + \hat{\hat{g}}_{002}\hat{\hat{z}}^2 + \hat{\hat{g}}_{003}\hat{\hat{z}}^3 \end{pmatrix} + \mathcal{O}\left(\left\|\hat{\hat{w}}, \hat{\hat{z}}\right\|^4\right),$$

where $\hat{\hat{f}}_{101} = \hat{f}_{101}$, $\hat{\hat{g}}_{110} = \hat{g}_{110}$, $\hat{\hat{g}}_{002} = \hat{g}_{002}$, and $\hat{\hat{g}}_{003} = \hat{g}_{003}$. Indeed, by imposing the condition $\widehat{F} \circ C(\hat{\hat{w}}, \hat{\hat{z}}) = C \circ \widehat{\widehat{F}}(\hat{\hat{w}}, \hat{\hat{z}})$ up to terms of order three, we get the linear system

$$\hat{g}_{110}\lambda_0 b_1 = \hat{f}_{210},$$

$$\hat{g}_{002}\lambda_0 b_1 - \hat{f}_{101}b_2 + \hat{\hat{f}}_{102} = \hat{f}_{102},$$

$$\hat{g}_{110}(b_1 + \overline{b_1}) - 2\hat{g}_{110}b_2 = -\hat{g}_{111},$$

in the variables $(b_1, b_2, \hat{\hat{f}}_{102})$, which is solvable due to the assumption in (37). This finishes the proof for $\alpha = 0$.

Step 3. Application of the implicit function theorem.

For α sufficiently small, by the implicit function theorem there exists a parameter-dependent transformation for which Eq. (36) takes the form

$$\begin{pmatrix} \hat{\hat{\lambda}}\hat{\hat{w}} + \hat{\hat{f}}_{101}\hat{\hat{w}}\hat{\hat{z}} + \hat{\hat{f}}_{102}\hat{\hat{w}}\hat{\hat{z}}^2 \\ \hat{\hat{g}}_{000} + \hat{\hat{z}} + \hat{\hat{g}}_{110}\hat{\hat{w}}\overline{\hat{\hat{w}}} + \hat{\hat{g}}_{002}\hat{\hat{z}}^2 + \hat{\hat{g}}_{003}\hat{\hat{z}}^3 \end{pmatrix} + \mathcal{O}\left(\left\|\hat{\hat{w}}, \hat{\hat{z}}\right\|^4\right), \tag{41}$$

where $\hat{\hat{\lambda}}(0) = \lambda_0$. To show that the implicit function theorem can be applied, the computations are elementary, but long and tedious.

Step 4. Final scalings and reparameterization.

A parameter-dependent scaling of the type

$$\hat{\hat{w}} = \sqrt{\frac{s}{\hat{\hat{g}}_{002}\hat{\hat{g}}_{110}}}\, w, \qquad \hat{\hat{z}} = \frac{1}{\hat{\hat{g}}_{002}} z, \tag{42}$$

where s is the sign of $\hat{\hat{g}}_{002}\hat{\hat{g}}_{110}$, is applied to (41). For simplicity we reuse the names of the starting variables. This yields

$$\begin{pmatrix} w \\ z \end{pmatrix} \mapsto \begin{pmatrix} (1 + \beta_2(\alpha))e^{i\beta_3(\alpha)}\lambda_0 w + a(\alpha)wz + b(\alpha)wz^2 \\ \beta_1(\alpha) + z + sw\overline{w} + z^2 + c(\alpha)z^3 \end{pmatrix} + \mathcal{O}(\|w, z\|^4).$$

The regularity of (38) is equivalent to that of the map $\alpha \mapsto \beta(\alpha)$. This means that β can be taken as new parameter.

A.2. The Takens normal form vector field for diffeomorphisms

In this section we present the version of the Takens theorem to be used in the proof of Theorem 1. This version is somewhat different with respect to the "classical" Takens theorem (see [61]: the latter is used in Section 3.2 to construct a vector field approximation for the fifth iterate of the model map G (3)). Indeed, the vector field T_F provided by the classical Takens theorem is such that all eigenvalues are zero: $\text{spec}\, DT_F(0, 0) = \{0\}$, since the semisimple part is factored out. On the other hand, to construct the model map G (3) we find it more convenient to start by a two-parameter HSN-family of vector fields on $\mathbb{R}^3 \times \mathbb{R}^2$, that is, a family X for which $\text{spec}\, DX(0, 0) = \{\pm i\omega_0, 0\}$, $\omega_0 \neq 0$. This motivates the version of Takens theorem reported here.

Let $F : \mathbb{R}^m \times \mathbb{R}^p \to \mathbb{R}^m \times \mathbb{R}^p$ be a diffeomorphism such that $F(0, 0) = (0, 0)$ and $\pi_p \circ F = \pi_p$, where $\pi_p : \mathbb{R}^m \times \mathbb{R}^p \to \mathbb{R}^p$ is the projection on the p-dimensional parameter space. Let S be the semisimple part of $DF(0, 0)$.

Theorem 7. *Let F be a family of diffeomorphisms of $\mathbb{R}^3 \times \mathbb{R}^p$, with $\pi_p \circ F = \pi_p$ such that*

$$F(0, 0) = 0 \quad and \quad \text{spec}\, DF(0, 0) = \{e^{i\omega_0}, e^{-i\omega_0}, 1\} \subset \mathbb{S}^1.$$

Suppose that the eigenvalue $\lambda_0 = e^{i\omega_0}$ satisfies the nonresonance conditions

$$\lambda_0^r \neq 1 \quad r = 1, \dots, k \tag{43}$$

for some integer $k \geq 3$. Then there exists a degree $k - 1$ polynomial vector field T_F on $\mathbb{R}^3 \times \mathbb{R}^p$, with $p \circ T_F = 0$, such that

$$F = T_F^1 + M, \tag{44}$$

where the remainder M is such that $\pi_p \circ M = \pi_p$ and $j^{k-1}M = 0$.

By (44), T_F^1 is an HSN-family of vector fields. In particular, if F is an HSN-family of diffeomorphisms, *i.e*, if $k \geq 4$ (compare (1)), then Theorem 7 implies that F can be written as a perturbation of the time-1 map T_F^1 of an HSN-family of vector fields. Moreover, the 3-jet of the perturbing term M in (44) is zero, which means that the Taylor expansion of M around $(0, 0)$ only contains terms of order at least four. The rest of this section is devoted to sketching the proof of Theorem 7.

Let $\mathcal{M}^n$ be the space of all homogeneous polynomial maps

$$P : \mathbb{R}^3 \times \mathbb{R}^p \to \mathbb{R}^3 \times \mathbb{R}^p$$

of degree n, with $\pi_p \circ P = 0$. We assume that the coordinates $x = (w, z, \alpha_1, \dots, \alpha_p)$ on $\mathbb{R}^3 \times \mathbb{R}^p$ are such that the semisimple part S of $DF(0, 0)$ is diagonal. A basis of $\mathcal{M}^n$ is given by all monomial maps

$$h(x)\frac{\partial}{\partial w}, \qquad h(x)\frac{\partial}{\partial z}, \qquad h(x) = w^{n_1}\overline{w}^{n_2}z^{n_3}\alpha_1^{n_4}\dots\alpha_p^{n_{p+3}}, \tag{45}$$

lexicographically ordered [25] and such that $n_1 + n_2 + n_3 + n_4 + \cdots + n_{p+3} = n$. Let X be a vector field on $\mathbb{R}^3 \times \mathbb{R}^p$ such that $\pi_p \circ X = 0$. Denote by $\phi(t, x)$ the flow of X at time t, starting at point x. For $r \geq 2$ write

$$\begin{aligned} X(x) &= X_1(x) + X_2(x) + \cdots + X_r(x) + \mathcal{O}(\|x\|^{r+1}), \\ \phi(t, x) &= \phi_1(t)x + \phi_2(t, x) + \cdots + \phi_r(t, x) + \mathcal{O}(\|x\|^{r+1}), \\ F(x) &= F_1 x + F_2(x) + \cdots + F_r(x) + \mathcal{O}(\|x\|^{r+1}) \end{aligned}$$

where $X_n, \phi_n(t, -)$, and F_n belong to $\mathcal{M}^n$ for all $n = 1, \dots, r$. The linear vector field X_1 is identified with its matrix representation in the given coordinates. The equation

$$j^r F = j^r \phi(1, -), \tag{46}$$

where the unknown is the vector field X, can be solved by induction on r. Indeed, system (46) is rewritten as

$$e^{X_1} = F_1,$$
$$\int_0^1 e^{-sX_1} X_n(e^{sX_1}x)ds = e^{-X_1} F_n(x) - \int_0^1 e^{-sX_1} Z^n(s, x)ds, \quad n = 2, \ldots, r, \tag{47}$$

where $Z^n(s, x) = \sum_{i=2}^{n-1} Z^{i,n}(s, x)$ and $Z^{i,n}(s, x)$ is given by

$$X_n(\phi(t, x)) = X_n(\phi_1(t)x) + \sum_{i=n+1}^{n} Z^{n,i}(t, x) + \mathcal{O}(\|x\|^{r+1}).$$

The key point is that system (47) is solvable. Indeed, let (S, N) be the semisimple-nilpotent decomposition of $DF(0, 0)$. Then in the given coordinates we have

$$S = \begin{pmatrix} S_1 & 0 \\ 0 & I_p \end{pmatrix}, \qquad N = \begin{pmatrix} 0 & N_1 \\ 0 & 0 \end{pmatrix}, \tag{48}$$

where $S_1 = \text{diag}\{\lambda_0, 1, \}$, I_p is the identity matrix of order p, and N_1 is the matrix of a linear operator $N_1 : \mathbb{R}^p \to \mathbb{R}^3$. Observe that we can write $S + N = S(I + S^{-1}N)$, and that both S and $I + S^{-1}N$ have a logarithm:

$$\log(S) = \text{diag}(i\omega_0, 0, 0, \ldots, 0), \qquad \log(I + S^{-1}N) = S^{-1}N,$$

the second equality since $N^2 = 0$. Therefore, the first equation of system (47) has the solution $X_1 = B + S^{-1}N$, where $B = \log(S)$, since

$$F_1 = DF(0, 0) = S + N = S(I + S^{-1}N) = \exp(B)\exp(S^{-1}N) = \exp(B + S^{-1}N).$$

To complete the sketch of proof for Theorem 7, it is enough to observe that by the next lemma the higher-order equations in system (47) are solvable for $n = 2, \ldots, k - 1$, given the assumptions in (43). This is the content of the next lemma.

Lemma 8. *Let $X_1 = B + S^{-1}N$, where S and N are defined in (48), while $B = \log(S)$. Suppose that (43) holds. Then the linear operator*

$$L^n : \mathcal{M}^n \to \mathcal{M}^n, \qquad L^n(P)(x) = \int_0^1 e^{-sX_1} P(e^{sX_1}x)ds$$

is invertible for all $n = 1, \ldots, k - 1$.

Proof. Let P be one of the monomials in the basis of $\mathcal{M}^n$ given in (45) and, to begin, suppose that

$$P(x) = h(x)\frac{\partial}{\partial w}, \quad \text{where } h(x) = w^{n_1}\overline{w}^{n_2}z^{n_3}\alpha_1^{n_4}\ldots\alpha_p^{n_{p+3}}.$$

In this setting, an important property is that the nilpotent part N (48) has no nonzero entries in the upper right block, which corresponds to phase-space variables (w, z). Therefore, by denoting $sS^{-1}N(x) = (f, \overline{f}, g, 0, \ldots, 0)$, the coefficients f and g only depend on the parameters $\alpha = (\alpha_1, \ldots, \alpha_p)$, on ω_0 and on s, but not on (w, z). Therefore we have

$$e^{sX_1}x = e^{sB}(I + sS^{-1}N)x = \left(\lambda_0^s(w + f), \overline{\lambda}_0^s(\overline{w} + \overline{f}), z + g, \alpha\right)$$
$$h(e^{sX_1}x) = \lambda_0^{s(n_1-n_2)}(w + f)^{n_1}(\overline{w} + \overline{f})^{n_2}(z + g)^{n_3}\alpha_1^{n_4}\ldots\alpha_p^{n_{p+3}}.$$

The expression for $h(e^{sX_1}x)$ is a sum of terms in which the monomial $h(x)$ self appears only once, since f and g do not depend on (w, z). In particular, this implies that the matrix of the operator L^n with respect to the basis in (45) (which is ordered lexicographically), is lower triangular. Therefore the eigenvalues of L^n have the form

$$v_w = \int_0^1 e^{i\omega_0(n_1-n_2-1)s}ds \quad \text{for } P(x) = h(x)\frac{\partial}{\partial w} \quad \text{or} \quad v_z = \int_0^1 e^{i\omega_0(n_1-n_2)s}ds \quad \text{for } P(x) = h(x)\frac{\partial}{\partial z}.$$

To check that the operator L^n is invertible, we have to show that all eigenvalues are nonzero. If $n_1 - n_2 = 1$ or $n_1 - n_2 = 0$, then $v_w = 1$ or $v_z = 1$, respectively. So there may be a zero eigenvalue only for $n_1 - n_2 \neq 0, 1$. In this case we have

$$v_w = \frac{\lambda_0^{n_1-n_2-1} - 1}{i\omega_0(n_1 - n_2 - 1)}, \qquad v_z = \frac{n_1 - n_2}{i\omega_0(n_1 - n_2)}.$$

Therefore L^n has a zero eigenvalue if and only if

$$\text{either} \quad \lambda^{n_1-n_2-1} = 1, \quad \text{with } n_1 - n_2 - 1 \neq 0 \tag{49}$$

$$\text{or} \quad \lambda^{n_1-n_2} = 1, \quad \text{with } n_1 - n_2 \neq 0. \tag{50}$$

However, given the nonresonance condition in the hypotheses, (49) can only happen if either $n_1 - n_2 \geq k + 2$ or $n_1 - n_2 \leq -k$, while (50) may be satisfied only if $|n_1 - n_2| \geq k + 1$. Since $|n_1 - n_2| \leq n$, there are no zero eigenvalues for all $n \leq k - 1$. This concludes the proof of Lemma 8. $\square$

Appendix B. Proofs

Proof of Theorem 1. Given a diffeomorphism $F_\alpha : \mathbb{R}^3 \to \mathbb{R}^3$, $\alpha \in \mathbb{R}^3$, as in the hypotheses, denote by $F : \mathbb{R}^3 \times \mathbb{R}^3 \to \mathbb{R}^3 \times \mathbb{R}^3$ the diffeomorphism given by $F(x, \alpha) = (F_\alpha(x), \alpha)$. By applying Theorem 7, one obtains an HSN-family T_F of parameter-preserving vector fields on $\mathbb{R}^3 \times \mathbb{R}^3$ such that $F = T_F^1 + M$, where $j^3 M = 0$. We now apply some of the normalising transformations described in [48, Sec. 8.5.1]. First, denote by J the (parameter-dependent) transformation bringing the linear part of T_F to Jordan normal form: that is $J_* T_F = (X_\alpha, 0)$, where X_α has the form

$$X_\alpha(w, z) = \begin{pmatrix} f_{000}(\alpha) + (\eta(\alpha) + i\nu(\alpha))w + \displaystyle\sum_{j+k+h \geq 2} f_{jkh}(\alpha)\, w^j \overline{w}^k z^h \\[4mm] g_{000}(\alpha) + \zeta(\alpha)z + \displaystyle\sum_{j+k+h \geq 2} g_{jkh}(\alpha)\, w^j \overline{w}^k z^h \end{pmatrix}, \tag{51}$$

where $f_{000}(0) = g_{000}(0) = \eta(0) = \zeta(0) = 0$, and $\nu(0) = \nu_0$. The open and dense conditions that the map F has to satisfy are obtained, implicitly, by imposing the conditions

$$g_{002}(0) \neq 0, \qquad g_{110}(0) \neq 0, \qquad \hat{\hat{f}}_{102}(0) \neq 0, \tag{52}$$

on the vector field X_α, where $\hat{\hat{f}}_{102}(0)$ is given by

$$\hat{\hat{f}}_{102}(0) = \text{Re}\left[\hat{f}_{102} + f_{101}\left(\frac{\text{Re}\,\hat{f}_{210}}{g_{110}} - \frac{3\hat{g}_{003}}{2g_{002}} + \frac{\hat{g}_{111}}{2g_{110}}\right) - \frac{\hat{f}_{210}g_{002}}{g_{110}}\right], \quad \alpha = 0, \tag{53}$$

and the coefficients $\hat{f}_{102}$, $\hat{f}_{210}$, $\hat{g}_{003}$, and $\hat{g}_{111}$ at $\alpha = 0$ are

$$\hat{f}_{102} = f_{102} + \frac{i}{\nu_0}\left[2f_{002}(f_{200} - g_{101}) - \frac{1}{2}|f_{011}|^2 - f_{110}\overline{f}_{002}\right],$$

$$\hat{f}_{210} = f_{210} + \frac{i}{\nu_0}\left[f_{110}f_{200} - \frac{1}{2}g_{200}f_{011} - |f_{110}|^2 - \frac{2}{3}|f_{020}|^2\right],$$

$$\hat{g}_{003} = g_{003} - \frac{2}{\nu_0}g_{101}\,\text{Im}\,f_{002}, \tag{54}$$

$$\hat{g}_{111} = g_{111} - \frac{2}{\nu_0}\left[g_{101}\,\text{Im}\,f_{110} + g_{200}\,\text{Im}\,f_{011}\right]$$

(compare with the coefficient $E(0)$ in [48, Eq. (8.73)]). Moreover, for the case of maps, one has to unfold the whole linear part of X_α: therefore, writing $\nu(\alpha) = \nu_0 + \nu_1(\alpha)$, with $\nu_1(0) = 0$, we assume that the derivative of the map

$$\alpha \mapsto (g_{000}(\alpha), \eta(\alpha), \nu_1(\alpha)) \tag{55}$$

is surjective at $\alpha = 0$. Denote by C the transformation bringing X_α to the Poincaré-Dulac normal form

$$\hat{X}_\alpha(w, z) = \begin{pmatrix} \hat{f}_{100}\hat{w} + \hat{f}_{101}\hat{w}\hat{z} + \hat{f}_{210}\hat{w}^2\overline{\hat{w}} + \hat{f}_{102}\hat{w}\hat{z}^2 \\[2mm] \hat{g}_{000} + \hat{g}_{110}\hat{w}\overline{\hat{w}} + \hat{g}_{002}\hat{z}^2 + \hat{g}_{111}\hat{w}\overline{\hat{w}}\hat{z} + \hat{g}_{003}\hat{z}^3 \end{pmatrix} + \mathcal{O}\left(\|\hat{w}, \hat{z}\|^4\right). \tag{56}$$

(see [48, Lemma 8.9]. The scaling of time as in [48, Eq. (8.74)] cannot be used: it would generate additional terms in the 3-jet of the time-one map of the vector field. Therefore, one can use a near-identity transformation as in [48, Eq. (8.74)]: it is easily seen that the terms $\hat{w}^2\overline{\hat{w}}$ and $\hat{w}\overline{\hat{w}}\hat{z}$ can be eliminated by a transformation of this form: denote D such a change of coordinates. Then we have

$$D_* C_* J_* T_F(\hat{w}, \hat{z}) = \begin{pmatrix} \hat{\hat{f}}_{100}\hat{\hat{w}} + \hat{\hat{f}}_{101}\hat{\hat{w}}\hat{\hat{z}} + \hat{\hat{f}}_{102}\hat{\hat{w}}\hat{\hat{z}}^2 \\[2mm] \hat{\hat{g}}_{000} + \hat{\hat{g}}_{110}\hat{\hat{w}}\overline{\hat{\hat{w}}} + \hat{\hat{g}}_{002}\hat{\hat{z}}^2 + \hat{\hat{g}}_{003}\hat{\hat{z}}^3 \end{pmatrix} + \mathcal{O}\left(\|w, z\|^4\right). \tag{57}$$

A scaling as in (42), denoted as S, brings the previous system to the form

$$\begin{pmatrix} (\beta_1(\alpha) + i(\omega_0 + \delta(\alpha)))w + awz + bwz^2 \\ \beta_2(\alpha) + sw\overline{w} + z^2 + cz^3 \end{pmatrix} + \mathcal{O}\left(\|w, z\|^4 \right).$$

The assumption of regularity of the map in (55) implies that the change of parameters given by $\alpha \mapsto (\beta_1(\alpha), \beta_2(\alpha), \delta(\alpha))$ is locally invertible: therefore, $(\beta_1, \beta_2, \delta)$ can be used as new parameters, obtaining the vector field $Z = (Z_{\beta_1, \beta_2, \delta}, 0)$, where $Z_{\beta_1, \beta_2, \delta}$ is defined in (5). Denote by H the diffeomorphism given by the composition of the previous transformations: $H = S \circ D \circ C \circ J$. Since $Z = H_* T_F$, one has $F = (H_*^{-1} Z)^1 + M = H^{-1} \circ Z^1 \circ H + M$. From this, (4) follows immediately. To conclude, we observe that the scaling as in [48, Eq. (8.74)] is used to eliminate the imaginary part of the coefficient of the term wz^2 and the term z^3 from the expression for Z, whereas the scaling of time at the end of the proof of Lemma 8.10 in [48] is used to normalize to unity the coefficient of wz^2; the fact that we refrain from performing these scalings of time explains the difference between (5) and (6). $\square$

Proof of Lemma 2. *Part* 1. Denote for simplicity $K(z) = \gamma\mu + az + \gamma z^2$ in the equations of $\widetilde{S}$ (16) and of S (13). A fixed point of the planar map $\widetilde{S}$ is given by a solution (r_0, z_0) of the equations

$$|1 - \gamma K(z_0)| = 1, \qquad r_0^2 = 1 - z_0^2.$$

Define $u = \gamma z$ and

$$M(u, \gamma) = |1 - \gamma K(u/\gamma)|^2 - 1 = (1 - \gamma^2\mu - a_1 u - u^2)^2 + a_2^2 u^2 - 1.$$

By the implicit function theorem, there exists a unique function $u(\gamma)$ defined for small γ and such that $M(u(\gamma), \gamma) = 0$, with $u(\gamma) = \mathcal{O}(\gamma^2)$. Indeed,

$$M(0, 0) = 0, \qquad \frac{\partial}{\partial u} M(0, 0) = -2a_1 \neq 0, \qquad \frac{\partial}{\partial \gamma} M(0, 0) = 0.$$

An explicit computation yields $u(\gamma) = -\gamma^2\mu/a_1 + \mathcal{O}(\gamma^3)$. Putting $z_0 = u(\gamma)/\gamma$ and $r_0^2 = 1 - z_0^2$ yields a fixed point (r_0, z_0) of $\widetilde{S}$.

The determinant of the derivative $D\widetilde{S}$ at (r_0, z_0), given by $1 + 2\gamma^2(\mu/a_1 - a_1) + \mathcal{O}(\gamma^3)$, is equal to 1 at $\mu = \mu^{\mathcal{H}}(\gamma) = a_1^2 + \mathcal{O}(\gamma)$, where the trace of $D\widetilde{S}$ at the fixed point is $2 + 2a_1\gamma^2 + \mathcal{O}(\gamma^3)$. There the derivative $D\widetilde{S}$ has two complex conjugate eigenvalues of modulus one. Moreover, $\det D\widetilde{S}$ is larger than 1 for $\mu < \mu^{\mathcal{H}}(\gamma)$ and smaller than 1 for $\mu > \mu^{\mathcal{H}}(\gamma)$. To check that the fixed point (r_0, z_0) undergoes a Hopf bifurcation at $\mu = \mu^{\mathcal{H}}$, the nondegeneracy conditions stated in *e.g.* [48] can be verified.
Part 2. The planar map $\widetilde{S}$ (16) up to terms of order $\mathcal{O}(\gamma^3)$ is

$$\begin{pmatrix} r \\ z \end{pmatrix} \overset{\widetilde{S}}{\mapsto} \begin{pmatrix} r \\ z \end{pmatrix} + \gamma \begin{pmatrix} -a_1 rz \\ 1 - r^2 - z^2 \end{pmatrix} + \gamma^2 \begin{pmatrix} r\left(-\mu + z^2\left(-1 + \dfrac{|a|^2}{2} - \dfrac{a_1^2}{2} \right) \right) \\ 0 \end{pmatrix} + \mathcal{O}(\gamma^3). \tag{58}$$

We look for a vector field $T_{\widetilde{S}}$ such that the time-γ map $T_{\widetilde{S}}^\gamma$ satisfies

$$T_{\widetilde{S}}^\gamma = \widetilde{S} + \mathcal{O}(\gamma^3). \tag{59}$$

The time-γ map of $T_{\widetilde{S}}$ is given by

$$T_{\widetilde{S}}^\gamma = id + \gamma T_{\widetilde{S}} + \frac{\gamma^2}{2}\dot{T}_{\widetilde{S}} + \mathcal{O}(\gamma^3). \tag{60}$$

Write $T_{\widetilde{S}} = V_1 + \gamma V_2$, where the vector fields V_j, $j = 1, 2$, are to be determined and may depend on γ. By combining (60) and (59) we have

$$T_{\widetilde{S}}^\gamma - id = \gamma V_1 + \gamma^2 V_2 + \frac{\gamma^2}{2}\dot{V}_1 = \widetilde{S} - id + \mathcal{O}(\gamma^3),$$

which yields

$$V_1 = \frac{1}{\gamma}(\widetilde{S} - id), \qquad V_2 = -\frac{1}{2}\dot{V}_1.$$

Then V_1 is easily derived from (58), while

$$\dot{V}_1 = \begin{pmatrix} -a_1(\dot{r}z + r\dot{z}) \\ -2(r\dot{r} + z\dot{z}) \end{pmatrix} + \mathcal{O}(\gamma) = \begin{pmatrix} -a_1(-a_1 rz^2 + r(1 - r^2 - z^2)) \\ -2(-a_1 r^2 z + z(1 - r^2 - z^2)) \end{pmatrix} + \mathcal{O}(\gamma).$$

By rearranging the terms of $V_1 + \gamma V_2$ having the same order in γ and by disregarding $\mathcal{O}(\gamma^2)$, we obtain (19). This proves point 2.

Part 3. For $\gamma = 0$ the vector field $T_{\widetilde{S}}$ (19) has an equilibrium $(r, z) = (1, 0)$. Since the derivative $DT_{\widetilde{S}}$ is invertible at $(r, z, \gamma) = (1, 0, 0)$, by the implicit function theorem there exist an equilibrium $(r, z)(\gamma) = (1, 0) + \mathcal{O}(\gamma)$ of (19) for all γ sufficiently small. Substitution of $(r, z)(\gamma)$ in (19) yields $(r, z)(\gamma) = (1, -\gamma\mu/a_1) + \mathcal{O}(\gamma^2)$.

For the stability of this equilibrium, observe that the derivative $DT_{\widetilde{S}}$ at $(r, z)(\gamma)$ is such that

$$\mathrm{Tr}(DT_{\widetilde{S}}) = \mathcal{O}(\gamma), \qquad \det(DT_{\widetilde{S}}) = -2a_1 + \mathcal{O}(\gamma).$$

So for γ small the eigenvalues of $DT_{\widetilde{S}}$ at $(r, z)(\gamma)$ are complex conjugate, and their real part is

$$\frac{1}{2}\mathrm{Tr}(DT_{\widetilde{S}}) = -z - \gamma a_1 + \mathcal{O}(\gamma^2) = \gamma(\mu/a_1 - a_1) + \mathcal{O}(\gamma^2).$$

Therefore the equilibrium $(r, z)(\gamma)$ undergoes a Hopf bifurcation at $\mu^{\mathcal{H}}(\gamma) = a_1^2 + \mathcal{O}(\gamma)$.

To find the heteroclinic connection, denote the terms of $T_{\widetilde{S}}$ (19) of order zero and one in γ by $T_{\widetilde{S},0}$ and $T_{\widetilde{S},1}$ respectively, *i.e.* write $T_{\widetilde{S}} = T_{\widetilde{S},0} + \gamma T_{\widetilde{S},1}$, where

$$T_{\widetilde{S},0} = \begin{pmatrix} -a_1 r z \\ 1 - r^2 - z^2 \end{pmatrix}, \qquad T_{\widetilde{S},1} = \begin{pmatrix} r\left(-\mu + \dfrac{a_1}{2} - \dfrac{a_1}{2}r^2 - bz^2\right) \\ z - (1 + a_1)r^2 z - z^3 \end{pmatrix},$$

with $b = 1 + \mathrm{Re}(a^2 + a)/2$. The vector field $T_{\widetilde{S},0}$ is integrable, with first integral

$$F(r, z) = \frac{a_1}{2}r^c\left(1 - \frac{r^2}{1 - a_1} - z^2\right), \qquad c = -\frac{2}{a_1},$$

and with integrating factor r^{c-1}. Moreover, $T_{\widetilde{S},0}$ has a heteroclinic connection given by the zero level set $F^{-1}(0)$. Multiplying $T_{\widetilde{S},0}$ by the integrating factor r^{c-1} gives a Hamiltonian vector field X_0. So the vector field

$$r^{c-1}T_{\widetilde{S}} = r^{c-1}T_{\widetilde{S},0} + \gamma r^{c-1}T_{\widetilde{S},1} = X_0 + \gamma X_1$$

is a perturbation of the Hamiltonian vector field X_0. The value of the parameter μ for which the heteroclinic connection of X_0 survives for $r^{c-1}T_{\widetilde{S}}$ is given by the zeroes of the integral

$$\int\int_{\mathrm{int}(F^{-1}(0))} \mathrm{Tr}(DX_1)\mathrm{d}r\mathrm{d}z. \tag{61}$$

This integral is written as a linear combination of three integrals I_{c-1}, I_{c+1}, I_{c+3}, where

$$I_\beta = \int_0^{\pi/2} \sin^\beta \theta \mathrm{d}\theta.$$

By using the recurrence relation $I_{\beta+1} = \frac{\beta}{\beta+1}I_\beta$, the integrals can be reduced to $I_{\beta-1}$, which is factored out. Therefore, up to a multiplicative constant the integral (61) is equal to

$$c\left(\mu - \frac{a_1}{2} + \frac{b}{3}\right) + \frac{c(2a_1(1 - a_1) - \frac{bc}{3} - 1)}{c + 3}.$$

From this we arrive at point 3.

Part 4. The rotation number on the invariant circle $\mathscr{C}$ of S (15) is determined by the dynamics in the ϕ-component, which only depends on all parameters and on z_0. Also notice that z_0 does not depend on ω, since the map $\widetilde{S}$ (16) does not. Moreover, the dynamics on $\mathscr{C}$ is always a rigid rotation, since all coefficients in the ϕ-component of S are constant along all orbits on $\mathscr{C}$.

We now determine parameter values for which the rotation number on $\mathscr{C}$ is exactly $2\pi/5$. Put $\omega = \omega_0 + \gamma\delta$, where $\omega_0/(2\pi) = 1/5$. Since the map S commutes with the axial rotation $R_\theta(w, z) = (\exp(i\theta)w, z)$ for all θ (and, in particular, for $\theta = \omega_0$), a point of period five on $\mathscr{C}$ is given by (r_0, ϕ_0, z_0), where ϕ_0 is a fixed point of

$$\phi \mapsto \phi + \gamma\delta + \arg(1 - \gamma K(z_0)) = \phi + \gamma\delta + \arctan\frac{-\gamma a_2 z_0}{\mathrm{Re}(1 - \gamma K(z_0))}. \tag{62}$$

By the implicit function theorem there exists a function $\delta_{1:5}(\gamma, \mu)$, with

$$\delta_{1:5}(\gamma, \mu) = -\frac{a_2\mu}{a_1}\gamma + \mathcal{O}(\gamma^2),$$

such that the map in (62) is the identity. Therefore, for parameter values $(\gamma, \mu, \delta_{1:5}(\gamma, \mu))$ *all* points of $\mathscr{C}$ have period five.

Part 5. This is a trivial consequence of the persistence of normally hyperbolic invariant manifolds, see [33,40]. $\quad\square$

Proof of Lemma 3. Define the auxiliary map $\widetilde{G} = (\widetilde{G}_w, \widetilde{G}_z)$, where the two components of $\widetilde{G}$ are

$$\widetilde{G}_w(w, z) = w[1 - \gamma(\gamma\mu + az + \gamma z^2)] + \gamma^3 e^{-i(\omega_0 + \gamma\delta)}\varepsilon_1 \overline{w}^4$$
$$\widetilde{G}_z(w, z) = z + \gamma(1 - |w|^2 - z^2).$$

Then we can write $G = R_{(\omega_0 + \gamma\delta)} \circ \widetilde{G}$ and $H = R_{\gamma\delta} \circ \widetilde{G}$. For any $c \in \mathbb{C}$ of modulus one we have

$$\widetilde{G}_w(cw, z) - c\widetilde{G}_w(w, z) = \gamma^3 e^{-i(\omega_0 + \gamma\delta)}(\overline{c}^4 - c)\varepsilon_1 \overline{w}^4 \quad \text{and} \quad \widetilde{G}_z(w, z) = \widetilde{G}_z(cw, z).$$

For either $c = e^{-i(\omega_0 + \gamma\delta)}$ or $c = e^{-i\gamma\delta}$ the term $\overline{c}^4 - c$ is of order $\mathcal{O}(\gamma)$. This implies

$$G(w, z) = R_{(\omega_0 + \gamma\delta)} \circ \widetilde{G} = \widetilde{G} \circ R_{(\omega_0 + \gamma\delta)} \bmod \mathcal{O}(\gamma^4),$$
$$H(w, z) = R_{\gamma\delta} \circ \widetilde{G} = \widetilde{G} \circ R_{\gamma\delta} \quad \bmod \mathcal{O}(\gamma^4), \quad \text{and, therefore,}$$
$$G^5(w, z) = \widetilde{G}^5 \circ R^5_{(\omega_0 + \gamma\delta)} = \widetilde{G}^5 \circ R^5_{\gamma\delta} = R^5_{\gamma\delta} \circ \widetilde{G}^5 = H^5 \bmod \mathcal{O}(\gamma^4).$$

This concludes the proof of Lemma 3. $\quad\square$

Proof of Theorem 4. The procedure is similar to the proof of Lemma 2, point 4. We search for a vector field T_H such that $T_H^\gamma = H + \mathcal{O}(\gamma^4)$. Write $T_H = V_1 + \gamma V_2 + \gamma^2 V_3$, where $V_j, j = 1, 2, 3$, may depend on γ. Then

$$T_H^\gamma - id = \gamma(V_1 + \gamma V_2 + \gamma^2 V_3) + \frac{\gamma^2}{2}(\dot{V}_1 + \gamma \dot{V}_2) + \frac{\gamma^3}{3!}\ddot{V}_1 + \mathcal{O}(\gamma^4).$$

Therefore the condition $T_H^\gamma - id = H - id + \mathcal{O}(\gamma^4)$ yields

$$V_1 = (H - id)/\gamma, \qquad V_2 = -\frac{1}{2}\dot{V}_1, \qquad V_3 = -\frac{1}{2}\dot{V}_2 - \frac{1}{6}\ddot{V}_1 = \frac{1}{12}\ddot{V}_1.$$

Denoting for simplicity $K(z) = \gamma\mu + az + \gamma z^2$ in the equation of H (21), we have

$$V_1 = \begin{pmatrix} w(\xi - e^{i\gamma\delta}K(z)) + \gamma^2 e^{-i\omega_0}\varepsilon_1 \overline{w}^4 \\ 1 - |w|^2 - z^2 \end{pmatrix}, \qquad \xi = \frac{e^{i\gamma\delta} - 1}{\gamma}$$

$$V_2 = -\frac{1}{2}\begin{pmatrix} w\left[(\xi - e^{i\gamma\delta}K(z))^2 - e^{i\gamma\delta}(a + 2\gamma z)(1 - |w|^2 - z^2)\right] \\ 2\left[|w|^2 \operatorname{Re}(\xi - e^{i\gamma\delta}K(z)) + z(1 - |w|^2 - z^2)\right] \end{pmatrix},$$

$$V_3 = \frac{1}{12}\begin{pmatrix} \ddot{w}\{[i\delta - az]^2 - a\dot{z}\} - 2aw\{\ddot{z}[i\delta - az] + \operatorname{Re}(\ddot{w}\overline{w}) + z\ddot{z}\} \\ 2\{2\operatorname{Re}(\ddot{w}\overline{w})(-a_1 z) - |w|^2 a_1\ddot{z} + \ddot{z}\dot{z} - 2z(\operatorname{Re}(\ddot{w}\overline{w}) + z\ddot{z})\} \end{pmatrix},$$

where $(\dot{w}, \dot{z})$ and $(\ddot{w}, \ddot{z})$ denote the components of V_1 and $\dot{V}_1$, respectively. Notice that terms of order $\mathcal{O}(\gamma)$ have already been discarded in V_3, since they give a contribution of order $\mathcal{O}(\gamma^3)$ in the vector field T_H and of order $\mathcal{O}(\gamma^4)$ in the time-γ map T_H^γ. By regrouping terms of the same order in γ in $T_H = V_1 + \gamma V_2 + \gamma V_3$, and by disregarding $\mathcal{O}(\gamma^3)$, we obtain (23)–(25). Part 1 of Theorem 4 is now proved. The proof of the remaining parts is straightforward. $\quad\square$

Proof of Theorem 5. *Part* 1. We search for equilibria of the vector field T_H (22) having cylindrical coordinates (r, ϕ, z) and occurring at parameter values (γ, μ, δ) such that

$$z = \mathcal{O}(\gamma), \qquad r = 1 + \mathcal{O}(\gamma^2), \qquad \delta = \mathcal{O}(\gamma), \tag{63}$$

compare with part two of Lemma 2. By (63), the terms U_w and U_z in (22) are of order $\mathcal{O}(\gamma)$. By disregarding all terms of order $\mathcal{O}(\gamma^3)$, the equilibrium condition $T_H = 0$ reads

$$-i\delta + \gamma\mu + az = \gamma^2\varepsilon_1 e^{-i(\omega_0 + 5\phi)} + \mathcal{O}(\gamma^3), \qquad r = 1 + \mathcal{O}(\gamma^2). \tag{64}$$

An additional variable z'' and a parameter δ'' are introduced:

$$z = \gamma z' + z''\gamma^2, \qquad \delta = \delta'\gamma + \delta''\gamma^2, \tag{65}$$

where z' and δ' are coefficients to be determined, which depend on μ but not on γ. The existence of the equilibria is proved by applying the implicit function theorem to an equation of the form $M(r, \phi, z'', \gamma, \mu, \delta'') = 0$, where the solutions (r, ϕ, z'') are functions of the parameters (γ, μ, δ''). The first equation of (64) is split in two, one equation for the terms in γ and another for terms of order $\mathcal{O}(\gamma^2)$. The equation for the terms in γ is divided in real and imaginary part, yielding

$$\mu + a_1 z' = 0, \qquad -\delta' + a_2 z' = 0, \tag{66}$$

which is directly solved for z' and δ'. The terms of order $\mathcal{O}(\gamma^2)$ give

$$-i\delta'' + az'' = \varepsilon_1 e^{-i(\omega_0 + 5\phi)} + \mathcal{O}(\gamma).$$

This is split in an equation for the modulus and another for the argument, which, together with the second of (64), yield the system

$$M(r, \phi, z'', \delta'', \gamma) = \begin{pmatrix} (-\delta'' + a_2 z'')^2 + (a_1 z'')^2 - \varepsilon_1^2 + \mathcal{O}(\gamma) \\ \omega_0 + 5\phi - 2k\pi + \arctan \dfrac{-\delta'' + a_2 z''}{a_1 z''} + \mathcal{O}(\gamma) \\ r - 1 + \mathcal{O}(\gamma^2) \end{pmatrix} = 0, \tag{67}$$

where $k = 0, \ldots, 4$. For $\gamma = 0$, this system has the solutions $(r_\pm, \phi_{k,\pm}, z''_\pm)$ where $r_\pm = 1$, $\phi_{k,\pm}$ has the expression in (28), and $z''_\pm$ is given in (29). For small γ the result holds since the derivative DM with respect to (r, ϕ, z'') is invertible, except when $-a_2\delta'' + |a|^2 z'' = 0$. This happens if and only if $\Delta = 0$ in (29), *i.e.* if the equilibria undergo saddle-node bifurcations, see the next part.

Part 2. To look for saddle-node bifurcations, the equation $\det(DT_H) = 0$ has to be added to the three deriving from the equilibrium condition $T_H = 0$. Moreover, δ'' has to be included as unknown together with (r, ϕ, z''). Up to and including terms of order two in γ we have

$$DT_H = \begin{pmatrix} i\delta - \gamma\mu - az - \dfrac{a}{2}\gamma & 4\varepsilon_1 e^{-i\omega_0}\gamma^2\overline{w}^3 - \dfrac{a}{2}\gamma w^2 & -w(a + 2\gamma z + a\gamma z) \\ -\overline{w}(1 + \gamma z) & -w(1 + \gamma z) & -2z - a_1\gamma \end{pmatrix} + \mathcal{O}(\gamma^3),$$

where we used that U_w (26) and U_z (27) are such that $DU_w = DU_z = \mathcal{O}(\gamma)$ for z and δ as in (65). Therefore, the saddle-node bifurcation condition reads

$$\det(DT_H) = 10(-a_2\delta + a_1\gamma\mu + |a|^2 z) + \mathcal{O}(\gamma^3) = 0, \tag{68}$$

which has to be solved together with (64). As in part 2, this system is first solved for the terms of order one in γ. In particular, Eq. (64) at order γ gives (66), which trivially satisfies (68) at order γ. The terms of order $\mathcal{O}(\gamma^2)$ give the system

$$M(r, \phi, z'', \delta'', \gamma) = \begin{pmatrix} -a_2\delta'' + |a|^2 z'' + \mathcal{O}(\gamma) \\ (-\delta'' + a_2 z'')^2 + (a_1 z'')^2 - \varepsilon_1^2 + \mathcal{O}(\gamma) \\ \omega_0 + 5\phi + \arctan \dfrac{-\delta'' + a_2 z''}{a_1 z''} - 2k\pi + \mathcal{O}(\gamma) \\ r - 1 + \mathcal{O}(\gamma^2) \end{pmatrix} = 0,$$

where $k = 0, \ldots, 4$. Notice that the first equation is the derivative of the second with respect to z''. This, of course, amounts to require that the second equation has a double solution, *i.e.* $\Delta = 0$ in (29). For $\gamma = 0$ this yields

$$\delta'' = \pm \frac{|a|}{|a_1|}\varepsilon_1, \qquad z'' = \pm \frac{a_2}{|a| |a_1|}\varepsilon_1.$$

Moreover, the derivative of M with respect to (r, ϕ, z'', δ'') is invertible at $\gamma = 0$, which allows application of the implicit function theorem. In particular (68) and the modulus of the first of (64) yield

$$a_2\gamma\mu + a_1\delta = \pm |a| \varepsilon_1,$$

which are the two lines $\mathcal{SN}^5_\pm$ (30).

Part 3 *and* 4. As in part 2, an equation has to be added to (67). Denote by (ν_1, ν_2, ν_3) the eigenvalues of DT_H. Then the characteristic polynomial of DT_H is

$$-\nu^3 + \mathrm{Tr}(DT_H)\nu^2 - \mathrm{Sim}(DT_H)\nu + \det(DT_H),$$

where $\mathrm{Sim}(DT_H) = \nu_1\nu_2 + \nu_1\nu_3 + \nu_2\nu_3$. The condition for a Hopf bifurcation is

$$\mathrm{Sim}(DT_H)\,\mathrm{Tr}(DT_H) = \det(DT_H) \neq 0. \tag{69}$$

In particular, we have (68) for $\det(DT_H)$ and

$$\mathrm{Tr}(DT_H) = -2(\gamma\mu + a_1 z + z + a_1\gamma) + \mathcal{O}(\gamma^3), \quad \mathrm{Sim}(DT_H) = -2a_1 + \mathcal{O}(\gamma^2).$$

Thereby, (69) reads

$$-3a_1\mu\gamma + z(2a_1^2 + 2a_1 - 5|a|^2) + a_1^2\gamma + 5a_2\delta = 0. \tag{70}$$

To determine the coordinates of the bifurcating equilibria, it is convenient to introduce the variable z'' and the parameters (μ', δ'') by

$$z = \gamma z' + z'' \gamma^2, \qquad \delta = \delta' \gamma + \delta'' \gamma^2, \qquad \mu = \mu^0 + \gamma \mu',$$

where (z', μ^0, δ') are constants to be determined, compare with (65). The system given by the equilibrium condition $T_H = 0$ together with (70) is split in two equations, one for the terms in γ and another for the terms of order $\mathcal{O}(\gamma^2)$. The terms in γ yield the system

$$\mu^0 + a_1 z' = 0, \qquad \delta' + a_2 z' = 0, \qquad -3a_1 \mu^0 + z'(2a_1^2 + 2a_1 - 5|a|^2) + a_1^2 + 5a_2 \delta' = 0,$$

which has the solution

$$z' = -a_1, \qquad \mu^0 = a_1^2, \qquad \delta' = -a_1 a_2.$$

The terms of order $\mathcal{O}(\gamma^2)$ yield

$$M \begin{pmatrix} r, \phi, z'' \\ \gamma, \mu', \delta'' \end{pmatrix} = \begin{pmatrix} -3a_1 \mu' + z''(2a_1^2 + 2a_1 - 5|a|^2) + 5a_2 \delta'' + \mathcal{O}(\gamma) \\ (-\delta'' + a_2 z'')^2 + (\mu' + a_1 z'')^2 - \varepsilon_1^2 + \mathcal{O}(\gamma) \\ \omega_0 + 5\phi + \arctan \dfrac{-\delta'' + a_2 z''}{\mu' + a_1 z''} - 2k\pi + \mathcal{O}(\gamma) \\ r - 1 + \mathcal{O}(\gamma^2) \end{pmatrix} = 0,$$

where $k = 0, \ldots, 4$. For $\gamma = 0$, the first equation yields

$$z'' = \frac{1}{c}(3a_1 \mu' - 5a_2 \delta''), \quad c = 2a_1 + 2a_1^2 - 5|a|^2. \tag{71}$$

Substitution of (71) into the second component of M gives (32). Conversely, from the second component of M we have (34). Substitution of (34) into (71) gives

$$\pm c\sqrt{\Delta'} = -2a_1 a_2(1 + a_1)\delta'' + 2a_1(a_1 - a_2^2)\mu'. \tag{72}$$

Since $c < 0$, this implies that the equilibrium with $\mathscr{P}_{k,+}^5$, corresponding to the "+" sign in the left hand side of (72), only can have a Hopf bifurcation when the right-hand side of (72) is negative. This gives inequality Eq. (33).

Part 5. The location of the $\mathcal{HSN}_{\pm}^5$ points is obtained as the solution of the system given by the equilibrium condition $T_H = 0$ (64), together with the saddle-node equation (68) and the Hopf condition (69). According to what has been said in part 3, (68) is equivalent to requiring $\Delta' = 0$ in (72). Therefore the solutions are obtained by setting (33) equal to zero and substituting in (31) and (32).

Part 6. The proof is carried out by means of an algebraic manipulator, *i.e.* a computer program that calculates the transformations in [48, Lemma 8.11] up to a finite order in the variables and parameters. The algebraic manipulator used in this proof is based on [42]. □

References

[1] V.S. Afrajmovich, L.P. Shil'nikov, On invariant two-dimensional tori, their disintegration and stochasticity, in: Methods of the Qualitative Theory of Differential Equations, Gor'kov. Gos. University, Gor'kij, 1983, pp. 3–26.

[2] V.I. Arnol'd, Mathematical Methods of Classical Mechanics, in: Springer GTM, vol. 60, 1980.

[3] V.I. Arnol'd, Geometrical Methods in the Theory of Ordinary Differential Equations, 2nd ed., Springer-Verlag, 1988.

[4] V.I. Arnol'd, V.S. Afrajmovich, Yu.S. Il'yashenko, L.P. Shil'nikov, I. Bifurcation Theory, in: V.I. Arnol'd (Ed.), Dynamical Systems V, in: Encyclopaedia of Mathematical Sciences, Springer-Verlag, 1982.

[5] D.G. Aronson, M.A. Chory, G.R. Hall, R.P. McGehee, Bifurcations from an invariant circle for two-parameter families of maps of the plane: A computer-assisted study, Comm. Math. Phys. 83 (3) (1982) 303–354.

[6] C. Baesens, J. Guckenheimer, S. Kim, R.S. McKay, Three coupled oscillators: Mode-locking, global bifurcations and toroidal chaos, Physica D 49 (3) (1991) 387–475.

[7] B.L.J. Braaksma, H.W. Broer, On a quasi-periodic Hopf bifurcation, Ann. Inst. H. Poincaré Anal. Non Linéaire 4 (2) (1987) 115–168.

[8] H.W. Broer, Formal normal forms for vector fields and some consequences for bifurcations in the volume preserving case, in: A. Dold, B. Eckmann (Eds.), Dynamical Systems and Turbulence, Warwick 1980, in: Springer LNM, vol. 898, 1980, pp. 54–74.

[9] H.W. Broer, G.B. Huitema, M.B. Sevryuk, Quasi-Periodic Motions in Families of Dynamical Systems, Order Amidst Chaos, in: Springer LNM, vol. 1645, 1996.

[10] H.W. Broer, G.B. Huitema, F. Takens, B.L.J. Braaksma, Unfoldings and bifurcations of quasi-periodic tori, Mem. AMS 83 (421) (1990) 1–175.

[11] H.W. Broer, R. Roussarie, Exponential confinement of chaos in the bifurcation sets of real analytic diffeomorphisms, in: H.W. Broer, B. Krauskopf, G. Vegter (Eds.), Global Analysis of Dynamical Systems, Festschrift Dedicated to Floris Takens for his 60th Birthday, IOP Publish., Bristol, 2001.

[12] H.W. Broer, R. Roussarie, C. Simó, On the Bogdanov–Takens bifurcation for planar diffeomorphisms, in: C. Perelló, C. Simó, J. Solà-Morales (Eds.), Equadiff 1991, Proceedings Western European Conference on Differential Equations, Barcelona 1991, World Scientific, London, 1993, pp. 81–92.

[13] H.W. Broer, R. Roussarie, C. Simó, Invariant circles in the Bogdanov–Takens bifurcation for diffeomorphisms, ETDS 16 (1996) 1147–1172.

[14] H.W. Broer, C. Simó, J.C. Tatjer, Towards global models near homoclinic tangencies of dissipative diffeomorphisms, Nonlinearity 11 (1998) 667–770.

H. Broer et al. / Physica D 237 (2008) 1773–1799

[15] H.W. Broer, C. Simó, R. Vitolo, Bifurcations and strange attractors in the Lorenz-84 climate model with seasonal forcing, Nonlinearity 15 (4) (2002) 1205–1267.
[16] H.W. Broer, C. Simó, R. Vitolo, The Hopf-saddle-node bifurcation for fixed points of 3D-diffeomorphisms: The Arnol'd resonance web, Bull. Belgian Math. Soc. Simon Stevin, 2008 (in press).
[17] H.W. Broer, C. Simó, R. Vitolo, The Hopf-saddle-node bifurcation for fixed points of 3D-diffeomorphisms: A computer assisted dynamical inventory, 2007 (in preparation).
[18] H.W. Broer, S.J. van Strien, Infinitely many moduli of strong stability in divergence free unfoldings of singularities of vector fields, in: J. Palis (Ed.), Geometric Dynamics, Proceedings, Rio de Janeiro 1981, in: Springer LNM, vol. 1007, 1983, pp. 39–59.
[19] H.W. Broer, F. Takens, Formally symmetric normal forms and genericity, Dynamics Reported 2 (1989) 36–60.
[20] H.W. Broer, F. Takens, F.O.O. Wagener, Integrable and non-integrable deformations of the skew Hopf bifurcation, Regular and Chaotic Dynamics 4 (2) (1999) 17–43.
[21] H.W. Broer, G. Vegter, Subordinate Shil'nikov bifurcations near some singularities of vector fields having low codimension, ETDS 4 (1984) 509–525.
[22] A. Chenciner, Bifurcations de points fixes elliptiques. I. Courbes invariantes, Publ. Math. IHES 61 (1985) 67–127.
[23] A. Chenciner, Bifurcations de points fixes elliptiques. II. Orbites périodiques et ensembles de Cantor invariants, Invent. Math. 80 (1985) 81–106.
[24] A. Chenciner, Bifurcations de points fixes elliptiques. III. Orbites périodiques de petites périodes et élimination résonnante des couples de courbes invariantes, Publ. Math. IHES 66 (1987) 5–91.
[25] S.-N. Chow, C. Li, D. Wang, Normal Forms and Bifurcation of Planar Vector Fields, Cambridge University Press, New York, 1994.
[26] M.C. Ciocci, A. Litvak-Hinenzon, H.W. Broer, Survey on dissipative kam theory including quasi-periodic bifurcation theory based on lectures by Henk Broer, in: J. Montaldi, T. Ratiu (Eds.), Geometric Mechanics and Symmetry: The Peyresq Lectures, in: LMS Lecture Notes Series, vol. 306, Cambridge University Press, ISBN-13: 9780521539579, 2005, pp. 303–355.
[27] L. Díaz, J. Rocha, M. Viana, Strange attractors in saddle cycles: Prevalence and globality, Inv. Math. 125 (1996) 37–74.
[28] F. Dumortier, S. Ibáñez, H. Kokubu, C. Simó, About the unfolding of a Hopf-zero singularity, 2007 (in preparation).
[29] F. Dumortier, R. Roussarie, J. Sotomayor, Generic 3-parameter families of vector fields on the plane, unfolding a singularity with nilpotent linear part. The cusp case of codimension 3, ETDS 7 (3) (1987) 375–413.
[30] F. Dumortier, R. Roussarie, J. Sotomayor, H. Zoladek, Bifurcations of Planar Vector Fields, in: LNM, vol. 1480, Springer, Berlin, 1991.
[31] E. Castellà, Sobre la dinàmica prop dels punts de Lagrange del sistema Terra-Luna, Ph.D. Thesis (in Catalan), Univ. of Barcelona, 2003.
[32] E. Castellà, À. Jorba, On the vertical families of two-dimensional tori near the triangular points of the Bicircular problem, Celestial Mech. 76 (2000) 35–54.
[33] N. Fenichel, Persistence and smoothness of invariant manifolds for flows, Indiana Univ. Math. J. 21 (1971/72) 193–226.
[34] P. Gaspard, Local birth of homoclinic chaos, Physica D 62 (1–4) (1993) 94–122.
[35] G. Gomez, J.M. Mondelo, C. Simó, Refined Fourier analysis: Procedures, error estimates and applications, preprint Universitat de Barcelona 2001.
[36] W. Govaerts, R. Khoshsiar Ghaziani, Y.A. Kuznetsov, H.G.E. Meijer, Numerical methods for two-parameter local bifurcation analysis of maps, SIAM J. Sci. Comput. 29 (2007) 2644–2667.
[37] J. Guckenheimer, P. Holmes, Nonlinear Oscillations, Dynamical Systems, and Bifurcations of Vector Fields, Springer-Verlag, 1983.
[38] A. Haro, R. de la Llave, A parameterization method for the computation of invariant tori and their whiskers in quasi-periodic maps: Numerical algorithms, Discrete and continuous dynamical systems-B 6 (6) (2006) 1261–1300.
[39] A. Haro, R. de la Llave, A parameterization method for the computation of invariant tori and their whiskers in quasi-periodic maps: Explorations and mechanisms for the breakdown of hyperbolicity, SIAM J. Appl. Dynam. Syst. 6 (1) (2007) 1–292.
[40] M.W. Hirsch, C.C. Pugh, M. Shub, Invariant Manifolds, in: Springer LNM, vol. 583, 1977.
[41] G. Iooss, J.E. Los, Quasi-genericity of bifurcations to high-dimensional invariant tori for maps, Comm. Math. Phys. 119 (1988) 453–500.
[42] À. Jorba, A methodology for the numerical computation of normal forms, centre manifolds and first integrals of hamiltonian systems, Experim. Math. 8 (1999) 155–195.
[43] À. Jorba, Numerical computation of the normal behaviour of invariant curves of n-dimensional maps, Nonlinearity 14 (2001) 943–976.
[44] V. Kirk, Breaking of symmetry in the saddle-node Hopf bifurcation, Phys. Lett. A 154 (1991) 243–248.
[45] B. Krauskopf, B. Oldeman, A planar model system for the saddle-node Hopf bifurcation with global reinjection, Nonlinearity 17 (4) (2004) 1119–1152.
[46] B. Krauskopf, B. Oldeman, Bifurcations of global reinjection orbits near a saddle-node Hopf bifurcation, Nonlinearity 19 (9) (2006) 2149–2167.
[47] B. Krauskopf, C. Rousseau, Codimension-three unfoldings of reflectionally symmetric planar vector fields, Nonlinearity 10 (1997) 1115–1150.
[48] Yu. Kuznetsov, Elements of Applied Bifurcation Theory, 2nd ed., Springer-Verlag, 1998.
[49] Yu. Kuznetsov, H.G.E. Meijer, Remarks on interacting Neimark–Sacker bifurcations, J. Difference Equ. Appl. 12 (10) (2006) 1009–1035.
[50] H.G.E. Meijer, Codimension 2 bifurcations of iterated maps, Ph.D. Thesis, University of Utrecht, 2006.
[51] J.M. Mondelo, Contribution to the study of fourier methods for quasi-periodic functions and the vicinity of the collinear libration points, Ph.D. Thesis, Universitat de Barcelona, 2001.
[52] A.I. Neishtadt, The separation of motions in systems with rapidly rotating phase, Prikladnaja Mat. Mekh. 48 (1984) 133–139.
[53] S. Newhouse, J. Palis, F. Takens, Bifurcations and stability of families of diffeomorphisms, Publ. Math. IHES 57 (1983) 5–71.
[54] S. Östlund, D. Rand, J. Sethna, E. Siggia, Universal properties of the transition from quasiperiodicity to chaos in dissipative systems, Physica D 8 (3) (1983) 303–342.
[55] J. Palis, W. de Melo, Geometric Theory of Dynamical Systems, An Introduction, Springer-Verlag, 1982.
[56] J. Palis, F. Takens, Hyperbolicity & Sensitive Chaotic Dynamics at Homoclinic Bifurcations, in: Cambridge Studies in Advanced Mathematics, vol. 35, Cambridge University Press, 1993.
[57] D. Ruelle, F. Takens, On the nature of turbulence, Comm. Math. Phys. 20 (1971) 167–192.
[58] F. Schilder, W. Vogt, S. Schreiber, H.M. Osinga, Fourier methods for quasi-periodic oscillations, Internat. J. Numer. Methods Eng. 67 (5) (2006) 629–671.
[59] C. Simó, On the use of Lyapunov exponents to detect global properties of the dynamics, in: F. Dumortier, H.W. Broer, J. Mahwin, S.M. Verduyn-Lunel (Eds.), Equadiff 2003, Proceedings International Conference on Differential Equations, Hasselt 2003, World Scientific, Singapore, ISBN: 981 256 169 2, 2005, pp. 714–719.
[60] C. Simó, H.W. Broer, R. Roussarie, A numerical survey on the Takens-Bogdanov bifurcation for diffeomorphisms, in: C. Mira, et al. (Eds.), European Conference on Iteration Theory 89, World Scientific, Singapore, 1992, pp. 320–334.
[61] F. Takens, Forced Oscillations and Bifurcations, in: Applications of Global Analysis 1, in: Communications of the Mathematical Institute Rijksuniversiteit Utrecht, vol. 3, 1974, reprinted in: H.W. Broer B. Krauskopf G. Vegter (Eds.), Global Analysis of Dynamical Systems: Festschrift Dedicated to Floris Takens for His 60th Birthday, IOP Publish. Bristol, 2001.

[62] F. Takens, A nonstabilizable jet of a singularity of a vector field, in: Dynamical Systems (Proc. Sympos., Univ. Bahia, Salvador, 1971), Academic Press, New York, 1973, pp. 583–597.

[63] F. Takens, Singularities of vector fields, Publ. Math. IHES 43 (1974) 47–100.

[64] F. Takens, F.O.O. Wagener, Resonances in skew and reducible quasi-periodic Hopf bifurcations, Nonlinearity 13 (2) (2000) 377–396.

[65] V.S. Varadarajan, Lie Groups, Lie Algebras, and their Representations, in: Springer GTM, 102, 1984.

[66] R. Vitolo, Bifurcations of attractors in 3D diffeomorphisms, Ph.D. Thesis, University of Groningen, 2003.

[67] R. Vitolo, H.W. Broer, C. Simo', The Hopf-saddle-node bifurcation for fixed points of 3D-diffeomorphisms, in: G. Gaeta, R. Vitolo, S. Walcher (Eds.), SPT 2007, Proceedings of the International Conference Symmetry and Perturbation Theory, Otranto, Italy 2–9, June 2007, World Scientific, ISBN: 978-981-277-616-7, 2007.

[68] F.O.O. Wagener, Semi-local analysis of the k:1 and k:2 resonances in quasi-periodically forced systems, in: H.W. Broer, B. Krauskopf, G. Vegter (Eds.), Global Analysis of Dynamical Systems. Festschrift Dedicated to Floris Takens for his 60th Birthday, IOP, Bristol, Philadelphia, 2001, pp. 113–129.

[69] F.O.O. Wagener, On the skew Hopf bifurcation, PhD Thesis, University of Groningen, 1998.